Universiteit Leiden
The Netherlands

SN 2009md: another faint supernova from a low-mass progenitor

Fraser, M.; Ergon, M.; Eldridge, J.J.; Valenti, S.; Pastorello, A.; Sollerman, J.; ... ; Turatto, M.

Citation

Fraser, M., Ergon, M., Eldridge, J. J., Valenti, S., Pastorello, A., Sollerman, J., ... Turatto, M. (2011). SN 2009md: another faint supernova from a low-mass progenitor. *Monthly Notices Of The Royal Astronomical Society*, *417*(2), 1417-1433. doi:10.1111/j.1365-2966.2011.19370.x

Version: Not Applicable (or Unknown)

License: Leiden University Non-exclusive license

Downloaded from: https://hdl.handle.net/1887/59559

Note: To cite this publication please use the final published version (if applicable).

Monthly Notices of the ROYAL ASTRONOMICAL SOCIETY

Mon. Not. R. Astron. Soc. **417,** 1417–1433 (2011) doi:10.1111/j.1365-2966.2011.19370.x

SN 2009md: another faint supernova from a low-mass progenitor

M. Fraser,[1★] M. Ergon,[2] J. J. Eldridge,[3] S. Valenti,[1] A. Pastorello,[1,4] J. Sollerman,[2] S. J. Smartt,[1] I. Agnoletto,[5] I. Arcavi,[6] S. Benetti,[5] M.-T. Botticella,[1] F. Bufano,[5] A. Campillay,[7] R. M. Crockett,[8] A. Gal-Yam,[6] E. Kankare,[9,10] G. Leloudas,[11] K. Maguire,[1,8] S. Mattila,[10,12] J. R. Maund,[11] F. Salgado,[7] A. Stephens,[13] S. Taubenberger[14] and M. Turatto[5]

[1]*Astrophysics Research Center, School of Mathematics and Physics, Queen's University Belfast, Belfast BT7 1NN*
[2]*Oskar Klein Centre, Department of Astronomy, AlbaNova, Stockholm University, 106 91 Stockholm, Sweden*
[3]*Institute of Astronomy, University of Cambridge, Madingley Road, Cambridge CB3 0HA*
[4]*Dipartimento di Astronomia, Universitá di Padova, Vicolo dell'Osservatorio 3, 35122 Padova, Italy*
[5]*INAF-Osservatorio Astronomico di Padova, Vicolo dell'Osservatorio 5, 35122 Padova, Italy*
[6]*Weizmann Institute of Science, Rehovot 76100, Israel*
[7]*Las Campanas Observatory, Carnegie Observatories, Casilla 601, La Serena, Chile*
[8]*Department of Physics (Astrophysics), University of Oxford, Keble Road, Oxford OX1 3RH*
[9]*Nordic Optical Telescope, Apartado 474, E-38700 Santa Cruz de La Palma, Spain*
[10]*Tuorla Observatory, Department of Physics and Astronomy, University of Turku, Väisäläntie 20, FI-21500, Finland*
[11]*Dark Cosmology Centre, Juliane Maries Vej 30, 2100 Copenhagen, Denmark*
[12]*Stockholm Observatory, Department of Astronomy, AlbaNova University Center, SE-106 91 Stockholm, Sweden*
[13]*Gemini Observatory, 670 North Aohoku Place, Hilo, HI 96720, USA*
[14]*Max-Planck-Institut fr Astrophysik, Karl-Schwarzschild-Str. 1, D-85748 Garching, Germany*

Accepted 2011 July 1. Received 2011 June 30; in original form 2010 November 16

ABSTRACT

We present adaptive optics imaging of the core-collapse supernova (SN) 2009md, which we use together with archival *Hubble Space Telescope* data to identify a coincident progenitor candidate. We find the progenitor to have an absolute magnitude of $V = -4.63^{+0.3}_{-0.4}$ mag and a colour of $V - I = 2.29^{+0.25}_{-0.39}$ mag, corresponding to a progenitor luminosity of log $L/\mathrm{L}_{\odot} \sim 4.54 \pm 0.19$ dex. Using the stellar evolution code STARS, we find this to be consistent with a red supergiant progenitor with $M = 8.5^{+6.5}_{-1.5}$ $\mathrm{M}_{\odot}$. The photometric and spectroscopic evolution of SN 2009md is similar to that of the class of sub-luminous Type IIP SNe; in this paper we compare the evolution of SN 2009md primarily to that of the sub-luminous SN 2005cs. We estimate the mass of ^{56}Ni ejected in the explosion to be $(5.4 \pm 1.3) \times 10^{-3}$ $\mathrm{M}_{\odot}$ from the luminosity on the radioactive tail, which is in agreement with the low ^{56}Ni masses estimated for other sub-luminous Type IIP SNe. From the light curve and spectra, we show the SN explosion had a lower energy and ejecta mass than the normal Type IIP SN 1999em. We discuss problems with stellar evolutionary models, and the discrepancy between low observed progenitor luminosities (log $L/\mathrm{L}_{\odot}$ ~4.3–5 dex) and model luminosities after the second dredge-up for stars in this mass range, and consider an enhanced carbon burning rate as a possible solution. In conclusion, SN 2009md is a faint SN arising from the collapse of a progenitor close to the lower mass limit for core collapse. This is now the third discovery of a low-mass progenitor star producing a low-energy explosion and low ^{56}Ni ejected mass, which indicates that such events arise from the lowest end of the mass range that produces a core-collapse SN (7–8 $\mathrm{M}_{\odot}$).

Key words: stars: evolution – stars: massive – supernovae: general – supernovae: individual: SN 2009md – galaxies: individual: NGC 3389.

★E-mail: mfraser02@qub.ac.uk

© 2011 The Authors

Downloaded from https://academic.oup.com/mnras/article/417/1/1417/984687
by Leiden University user
on 23 November 2017

1 INTRODUCTION

Core-collapse supernovae (SNe) mark the endpoint of stellar evolution for stars more massive than ∼8 $M_\odot$ (Heger et al. 2003; Eldridge & Tout 2004; Siess 2007; Poelarends et al. 2008). When a star more massive than this exhausts its nuclear fuel, it can no longer support itself against gravitational collapse. The ensuing collapse, and subsequent explosion of the progenitor star, gives rise to the SN's spectacular display. The fact that the progenitors of core-collapse SNe are massive, and hence luminous, gives a realistic prospect of successfully recovering them in high-resolution archival data (see Smartt 2009, for a review). Since the first identification of a core-collapse SN progenitor, for SN 1987A in the Large Magellanic Cloud (West et al. 1987; White & Malin 1987), there have been numerous direct detections of SN progenitors (e.g. SN 1993J, Aldering, Humphreys & Richmond 1994; SN 2004A, Hendry et al. 2006; SN 2004et, Li et al. 2005; Crockett et al. 2011; SN 2005cs, Maund, Smartt & Danziger 2005; Li et al. 2006; SN 2008cn, Elias et al. 2009). Of particular interest is the family of sub-luminous Type IIP SNe (Pastorello et al. 2004), which are typified by fainter absolute magnitudes, lower expansion velocities and smaller ejected ^{56}Ni masses than the canonical Type IIP SNe. In recent years, there has been some debate in the literature as to the precise nature of these events, and whether they represent the collapse of a low-mass (∼9 $M_\odot$) star with an O–Ne–Mg core (Kitaura, Janka & Hillebrandt 2006), or a high-mass (∼25 $M_\odot$) star with the formation of a black hole, possibly by the fallback of material on to an accreting proto-neutron star (Turatto et al. 1998; Zampieri et al. 2003). The recovery of progenitors in archival data can help determine which scenario is (or whether both, or neither, are) correct.

SN 1997D was the prototype of this class of sub-luminous Type IIP SNe; at discovery the SN had line velocities of ∼1200 km s^{-1}, and at later epochs a low ejected nickel mass was measured from the radioactive tail (Benetti et al. 2001). Turatto et al. (1998) claimed SN 1997D resulted from the collapse of a high-mass (26 $M_\odot$) progenitor. This was based, however, on SN modelling, which gives consistently higher masses than found from progenitor modelling (Maguire et al. 2010b). Since the discovery of SN 1997D about a dozen sub-luminous Type IIP SNe have been discovered and classified (Pastorello et al. 2004; Spiro & Pastorello 2009). Out of these, four have either progenitor detections or useful upper mass limits. SN 2005cs was the first sub-luminous Type IIP SN for which a 6–8 $M_\odot$ progenitor was detected (Maund et al. 2005; Li et al. 2006; Eldridge, Mattila & Smartt 2007). The SN displayed a low expansion velocity, and had a faint absolute magnitude of $V = -14.75$ mag (Pastorello et al. 2006, 2009) and a low ^{56}Ni mass. For SN 2008bk (Pignata et al., in preparation) another low-mass, red supergiant progenitor of 8.5 ± 1.0 $M_\odot$ was identified by Mattila et al. (2008) in optical and near-infrared (NIR) pre-explosion imaging. The sub-luminous SNe for which we have a progenitor mass limit are SN 1999br (Filippenko 1999; Pastorello et al. 2004), where Maund et al. (2005) give a progenitor mass <12 $M_\odot$ (more recently revised to $M < 15$ $M_\odot$ by Smartt et al. 2009), and SN 2006ov, where a progenitor limit $M < 10$ $M_\odot$ was set by Crockett et al. (2011). From the low luminosities of the progenitors, we can rule out very massive stars, and bright, low-mass, super-asymptotic giant branch (SAGB) stars as the source of a significant fraction of these events.

In light of this, the detection of the progenitor of another sub-luminous Type IIP, coupled with the detailed monitoring and follow-up observations needed to understand the explosion, is of considerable interest. Understanding the nature of faint SNe, and how stars at the lower extremum of Type II SN progenitor masses give rise to them, can even help shed light on other questions, such as the upper mass limit for the formation of SAGB stars (e.g. Siess 2007; Pumo et al. 2009). Sub-luminous SNe may also nucleosynthesize different relative fractions of elements, and so influence the observed abundances in subsequent generations of stars (Tsujimoto & Shigeyama 2003).

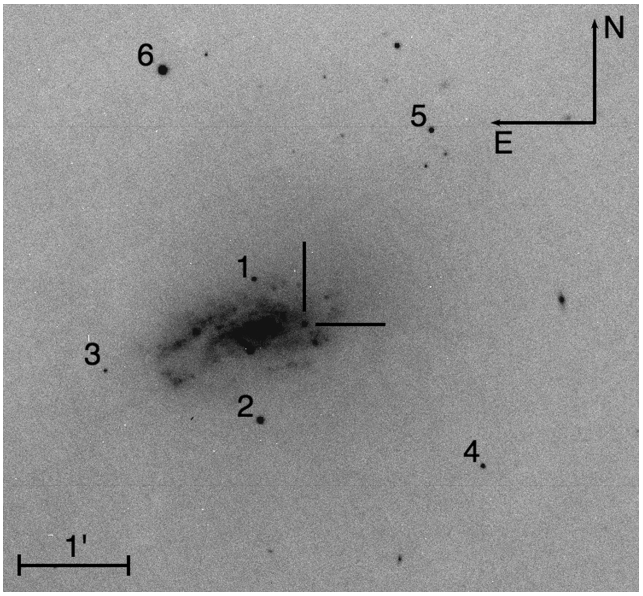

Figure 1. 5-s unfiltered acquisition image of NGC 3389, obtained on 2009 December 07 with the NOT+ALFOSC. The location of SN 2009md is indicated with cross marks; sequence stars used to calibrate optical photometry are numbered according to Table 2.

SN 2009md was found at an unfiltered magnitude of 16.5 mag by K. Itagaki (Nakano 2009) in the spiral galaxy NGC 3389 on 2009 December 4. The location of the SN is shown in Fig. 1. Sollerman et al. (2009) obtained a spectrum of the SN on 2009 December 7 with the Nordic Optical Telescope (NOT) + Andalucia Faint Object Spectrograph and Camera (ALFOSC), and classified it as a young Type IIP. To constrain the explosion epoch, we used a 120-s i'-band image of NGC 3389 from P.-A. Duc, which was taken on 2010 November 19 with the Canada–France–Hawaii Telescope (CFHT) + MegaCam. The data were reduced by the ELIXIR pipeline; the SN is not visible in the image at this epoch to a limiting magnitude of $i' > 23.4$.

We also used the SN spectrum comparison tool GELATO (Harutyunyan et al. 2008) to compare the earliest spectrum available of SN 2009md, from 2009 December 7, to those of other Type II SNe, finding matches with Type II SNe at phases of +3 to +10 d. We have hence adopted an explosion epoch of 2009 November 27 (MJD 55162), with an uncertainty of ±8 d. This epoch will be used as a reference throughout the paper.

The rest of this paper is laid out as follows. In Section 2, we discuss the archival data covering the location of SN 2009md, our progenitor detection and analysis. We also characterize the host galaxy, and estimate metallicity and distance. Section 3 deals with photometry and spectra of the SN itself; we also present a bolometric light curve for SN 2009md and an estimate of the ejected ^{56}Ni mass. In Section 4 we present further discussion and analysis of the SN. We verify the distance to NGC 3389 with the standard candle method for Type IIP SNe, discuss how changes to stellar evolutionary models may help ameliorate the discrepancy between

Downloaded from https://academic.oup.com/mnras/article-abstract/417/2/1417/984687
by Leiden University user
on 23 November 2017

the observed low luminosity of the progenitor of SN 2009md and the final luminosities found from models, estimate the explosion energy, and discuss the properties of the family of sub-luminous Type IIP SNe.

2 HOST GALAXY AND PROGENITOR CANDIDATE

2.1 NGC 3389

The host galaxy, NGC 3389, has a distance modulus $\mu = 31.85 \pm 0.15$ mag from its recessional velocity (1712 km s^{-1}, value from NED[1]) after correcting for infall on Virgo, Great Attractor (GA) and Shapley. Terry, Paturel & Ekholm (2002) find $\mu = 31.43 \pm 0.14$ mag from the 'sosies' method, while the Tully–Fisher relation gives $\mu = 31.76 \pm 0.8$ mag (Tully 1988). We took the mean of the three measurements (weighted by the inverse of the associated uncertainty for each method) to obtain a distance modulus $\mu = 31.64 \pm 0.21$ mag. The error in the distance modulus was calculated as the range of the three values about the mean.

Ideally, to estimate the metallicity at the SN location we would use a measurement of the ratio of the [O II] and [O III] to Hβ lines in an H II region close to the SN (Bresolin 2008). Unfortunately, we do not have such a measurement for NGC 3389.[2] Hence, we are forced to rely upon an estimated characteristic metallicity for the host, based on its absolute magnitude and a radial metallicity gradient, of $12 + \log(\mathrm{O/H}) = 8.96 \pm 0.04$ dex from the calibration of Boissier & Prantzos (2009). We note that this error does not take into account the intrinsic scatter in the calibration of Boissier & Prantzos, which is significant. As the determined metallicity is close to the solar value (Asplund et al. 2009), we have used solar metallicity evolutionary tracks in Section 2.6.

2.2 Archival data

NGC 3389 was observed with the Wide Field and Planetary Camera 2 (WFPC2) on board the *Hubble Space Telescope* (*HST*) on 2005 May 20 (∼1650 d before explosion). Eight images were obtained in each filter, with total exposure times of 2.81 h in $F606W$ and 2.75 h in $F814W$. The location of SN 2009md fell on the WF2 chip, which has a pixel scale of 0.1 arcsec pixel^{-1}. Reprocessed data were downloaded from the European Southern Observatory (ESO) archive,[3] these data have up-to-date calibrations applied by the On-The-Fly (OTF) pipeline.

The 3.6-m New Technology Telescope (NTT) observed the site of SN 2009md on 2002 March 25 in the H and K_s filters with the NIR camera and spectrograph Son of Isaac (SOFI), which has a pixel scale of 0.29 arcsec pixel^{-1}. The K_s filter data had a total exposure time of 480 s (comprising eight separate frames, each with 10 × 6 s sub-integrations), while the H filter data had a total exposure time of 360 s (eight frames, each with 3 × 15 s sub-integrations).[4]

2.3 Alignment and photometry

We obtained a K-band image of SN 2009md on 2010 February 27 (MJD 55254) with Near Infrared Imager and Spectrometer (NIRI)+Altitude Conjugate Adaptive Optics for the Infrared (ALTAIR) on the Gemini North telescope as part of our progenitor identification program.[5] We used the f/32 camera on NIRI (Hodapp et al. 2003) which has a 0.022 arcsec pixel scale across a 22.4 × 22.4 arcsec^2 field of view. ALTAIR is the adaptive optics system on Gemini, and provides the ∼0.1 arcsec resolution needed for precision astrometry. As the SN was too faint to use as a natural guide star for ALTAIR, we used the laser guide star (LGS) to guide for high-order corrections, and the SN itself for tip-tilt corrections.

As the location of the SN is in a crowded field, we obtained off-source images which were then used for sky subtraction of the on-source images. Each image consisted of a 60 s integration (comprising 2 × 30 s coadds), and after removing bad frames we were left with 1860 s on source. Data were reduced using the GEMINI NIRI routines within IRAF[6]; the basic steps consisted of creating a master flat-field by median combining the appropriate images, followed by masking of bad pixels and division by the master flat for both on- and off-source images. The sky images taken immediately before and after each series of on-source images were median combined to make a sky image for that sequence. Finally, the sky-subtracted on-source frames were median combined to create the final, reduced image.

After aligning the pre-explosion (WFPC2 $F814W$) and post-explosion (NIRI K) images according to the World Coordinate System (WCS), we identified 32 sources common to both images. The coordinates of these sources were measured with the IRAF PHOT task using the centroid centring algorithm. The list of matched coordinates was then used as input to the IRAF GEOMAP task to derive a geometric transformation between the two images, allowing for translation, rotation and independent scaling in the x- and y-axes. 10 sources were rejected at this stage, as they were outliers of more than one NIRI pixel from the fit. With 22 sources remaining though, we can be confident of not over-fitting the data. The rms error in the fit was 14 mas.

The coordinates of the SN were measured in the NIRI image with the three different centring algorithms offered by the PHOT task: centroid, Gaussian and optimal filtering. The SN is by far the brightest source in the NIRI image, and hence there is no risk of nearby sources within the centring box influencing the centring algorithm. We took the mean of the three centring algorithms as the true (NIRI) pixel coordinates of the SN, with the range (3 mas) as the error. We then transformed these coordinates to WFPC2 pixel coordinates using the previously determined transformation.

We can immediately identify a progenitor candidate close to the transformed SN position in the WFPC2 image. Precisely measuring its pixel coordinates is more problematic, as a bright source to the south west will affect the centring algorithms used, introducing a systematic error in all our results. To avoid this, we simultaneously fit a point spread function (PSF) to both the progenitor candidate and all nearby sources, and used the centre coordinates as determined by this fitting process as the progenitor coordinates. We used TINY TIM (Kirst & Hook 2004) to model a PSF for the chip and pixel coordinates of the progenitor in the WFPC2 $F814W$ filter image. We then used the ALLSTAR task within the IRAF DAOPHOT package to fit

[1] $H_0 = 73$ km s^{-1}Mpc^{-1}.

[2] We note that there is published photometry of H II regions in NGC 3389 (Abdel-Hamid, Lee & Notni 2003), with two regions close to the position of SN 2009md. The closer region, H14, has a projected distance ∼2 arcsec, the more distant, H16, has a distance of ∼3.5 arcsec. Both regions have a similar luminosity, $10^{38.4}$ erg s^{-1}.

[3] http://archive.eso.org

[4] Images from the Subaru Telescope + SuprimeCam and the 3.6-m ESO telescope + ESO Faint Object Spectrograph and Camera (EFOSC2) were also examined, but were found to be unusable.

[5] GN-2010A-Q-54.

[6] http://iraf.noao.edu/

Downloaded from https://academic.oup.com/mnras/article-abstract/417/2/1417/984687
by Leiden University user
on 23 November 2017

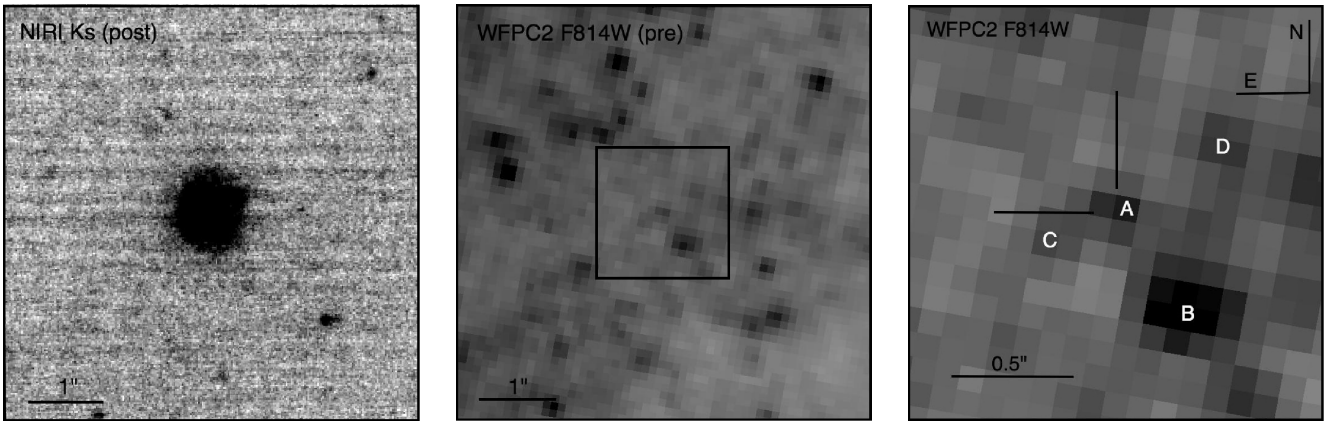

(a) Section of Gemini NIRI post-explosion image, centered on the SN.

(b) Section of HST WFPC2 pre-explosion image, centered on the SN location. A blow up of the central region (indicated by a black square is shown in panel (c).

(c) Blow-up of progenitor (Source A, at intersection of lines) together with nearby sources (B, C and D).

Figure 2. Pre- and post-explosion images used for progenitor identification.

the PSF to the pre-explosion WFPC2 image. Fitting the progenitor candidate (source A in Fig. 2) and the nearby bright source (B), together with two fainter sources (marked C and D) we find the progenitor candidate to be 16 mas from the transformed SN coordinates. Estimating the error in the progenitor coordinates is also difficult as the error introduced by the nearby bright source will affect all three centring algorithms in PHOT similarly. To overcome this, we subtracted the bright nearby source (B) using the model PSF created previously, and measured the position of the progenitor using a 3×3 pixel centring box. While this is a small region to centre over, ∼75 per cent of the flux of our model PSF is within these 9 pixels, and in a region where the background sky is varying on small scale it is necessary to use a small centring box. As before, the range of positions given by the three centring algorithms within PHOT was taken as the error, which in this case was 15 mas.

Adding the uncertainties in progenitor (15 mas) and SN (3 mas) location in quadrature with the rms error in the transformation (14 mas), we find a total error of 21 mas. The progenitor candidate and SN are separated by 16 mas, which is comfortably within the combined fit uncertainty, and so we find the progenitor candidate and SN to be coincident. The progenitor candidate is shown in Fig. 2.

To perform photometry on the identified progenitor candidate, we used the HSTPHOT package (Dolphin 2000a), which is a dedicated package optimized for photometry of under-sampled WFPC2 images. HSTPHOT incorporates up-to-date corrections for charge transfer efficiency (CTE), and can convert magnitudes from the *HST* flight system to the standard *UBVRI* system (Dolphin 2000b, 2009). As HSTPHOT cannot be run on drizzled images, we obtained the original individual images in each filter from the Multimission Archive at the Space Telescope Science Institute (MAST) archive at Space Telescope Science Institute (STScI). All images were masked for bad pixels based on their associated data quality image; cosmic rays were detected and masked with a median filter.

Using HSTPHOT, we found the progenitor magnitude to be $m_{F606W} = 26.736 \pm 0.15$ mag and $m_{F814W} = 24.895 \pm 0.08$ in the *HST* flight system, corresponding to a Johnson–Cousins magnitude of $m_V = 27.32 \pm 0.15$ mag and $m_I = 24.89 \pm 0.08$ mag (using the transformations of Dolphin 2000b, 2009).

As a check on the accuracy of our photometry, we used the TINY TIM package to create a WFPC2 PSF, appropriate for the chip, progenitor coordinates on the chip and filter for the pipeline drizzled $F814W$ image, which we used to identify our progenitor. PSF-fitting photometry was then simultaneously performed on our progenitor candidate, and on all bright nearby sources using the IRAF DAOPHOT package. The zero-point for the photometry was taken from the header; we multiplied by PHOTFLAM to obtain a flux, and then used the standard zero-point for WFPC2 to convert this value to a magnitude. We found a magnitude in the $F814W$ filter for the progenitor which was 0.1 mag brighter than that returned by HSTPHOT, which is comparable to our uncertainty.

We also repeated the same procedure for eight sources, of comparable magnitude to our progenitor candidate, that were detected both by HSTPHOT and by DAOPHOT. In all cases DAOPHOT returned a magnitude that was brighter than HSTPHOT. The mean difference in brightness was 0.2 mag, with a standard deviation of 0.1 mag. The reason for this systematic discrepancy is unclear, although we stress that it does not affect the results of this paper in any significant sense, as the discrepancy is comparable to the uncertainty of the output of HSTPHOT. We are inclined to favour the values returned by HSTPHOT as the package is optimized specifically for undersampled WFPC2 images. As a more qualitative indicator of the accuracy of our photometry, the supergiant sequence shown in Fig. 4 appears reasonable, in that we do not see any gross discrepancies with the standard sequence that would indicate there is a systematic error in our photometry.

While the SN and progenitor candidate are spatially coincident to within the errors, in deep, crowded fields in such a nearby galaxy we must be wary of a chance alignment between the SN and an unrelated source. We will argue against this being the case using several independent lines of reasoning. First, we consider the likelihood of a chance alignment based simply on the number of detected sources in the field. While we find a total error of ∼21 mas in the alignment for SN 2009md, even if we found a source coincident to within a ∼40 mas error in alignment, we would likely consider this a plausible progenitor candidate. Hence, we took a region around the SN covering 36 arcsec^2, and used the number of sources detected by HSTPHOT at a significance of $\geq 5\sigma$ (428 objects), together with an arbitrary 'association' distance of 40 mas around each source to calculate a probability of a chance alignment, which we find to be 6 per cent. This is a very rough estimate, as some of the regions around each source will overlap, reducing this probability. Of

Downloaded from https://academic.oup.com/mnras/article-abstract/417/2/1417/984687
by Leiden University user
on 23 November 2017

course, if we found a coincident source at the 4σ level, or a source 41 mas from the SN, we would likely consider it an interesting association, so the values adopted in this calculation are somewhat arbitrary. None the less, 6 per cent is probably a sensible estimate of a chance alignment for any source with the SN. We can further reduce this probability by considering the likelihood of finding a source coincident with the SN, and with a colour redder than some set value. If we repeat the calculation, but only for sources with a $V - I$ colour greater than 1.25 mag, corresponding to a supergiant of spectral type K0 or later, we find a likelihood of a chance alignment of <2 per cent.

2.4 SOFI data

The SOFI data were downloaded from the ESO archive, together with appropriate calibration frames (flat fields and dark frames) taken on the same night. The data were reduced using standard IRAF tasks. Subtraction of the flux from the sky is crucial in the NIR; unfortunately in this case there were no off-source sky-frames, and the dithers between the on-source frames were too small to allow a clean sky image to be constructed. We have created a median combined sky image using the on-source science frames, and subtracted this from each individual frame using the IRAF XDIMSUM package. The individual reduced science frames were then aligned and median combined to produce a final, reduced image, which is shown in Fig. 3.

We registered the H and K_s pre-explosion images to the post-explosion NTT+EFOSC2 R-band image from 2010 January 22, as the field of view covered by the post-explosion NIRI image was too small to identify sufficient numbers of common sources. The same basic procedure was followed as when aligning the WFPC2 and NIRI images, 15 sources common to both images were identified. The positions of these reference stars were measured in both frames with IRAF PHOT. The list of matched coordinates was then used with IRAF GEOMAP to derive a transformation, allowing for translation, rotation and a scaling factor. Two sources were rejected as outliers from the fit, the final rms error in the transformation was 0.541 pixels, which corresponds to 130 mas for the 0.24 arcsec binned pixels of EFOSC2. As before, we measured the position of the SN in the EFOSC2 image using the three centring algorithms within PHOT, and find a range of 4 mas between the measurements. Using the GEOXYTRAN and the derived transformation, we transformed the measured coordinates of the SN to the pre-explosion SOFI image.

There is no obvious source present at the location of SN 2009md in either the H- or K_s-band pre-explosion image. A non-detection is still of interest, as we can use it to constrain the magnitude of the progenitor in the NIR. A photometric zero-point of $ZP_{K_s} = 23.9$ mag was determined for the K_s image using PSF-fitting photometry with reference to catalogued Two Micron All-Sky Survey (2MASS) sources in the field. As the main source of noise in the NIR is from the bright sky background; this is the dominant factor in our limiting magnitude. We measured the standard deviation of the sky background at the SN position using the IRAF IMEXAM task, and found it to be ~3 ADU. Assuming that the central pixel of a detected source at confidence level of 3σ will have a flux at centre of three times the standard deviation, we calculated the magnitude of a PSF with a central pixel 3σ above the background, at the location of the SN (and using the same aperture size as used for the sequence stars). We find a limiting magnitude of $K_s > 19.4$ mag. The H filter image did not yield a useful stringent limit.

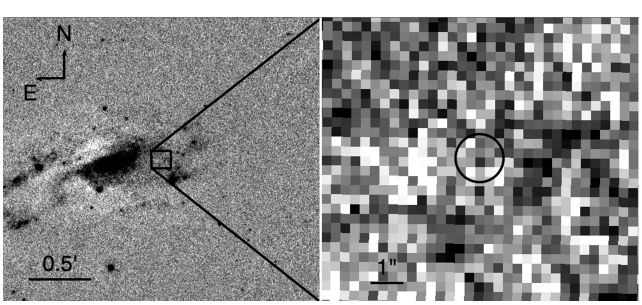

Figure 3. Subsections of pre-explosion NTT SOFI image of NGC 3389, taken with the K_s filter. Right-hand panel shows a magnified portion of the field (indicated by the box). The field is centred on the SN position, as discussed in the text. The circle corresponds to five times the positional uncertainty in the transformation and SN coordinates.

2.5 Extinction estimates

The foreground extinction towards NGC 3389 was taken, via NED,[7] from the (Schlegel, Finkbeiner & Davis 1998) dust maps, which give a colour excess $E(B - V) = 0.027$ mag. Estimating the total line-of-sight extinction to the SN is more difficult as there is not a single technique which gives reliable results. Turatto, Benetti & Cappellaro (2003) give an empirical relation between the equivalent width of the Na I doublet, EW(Na I D), at 5890 and 5896 Å and the colour excess $E(B - V)$. The Na I D observed in the spectrum of SN 2009md is a blend of the contribution from the host galaxy and the Milky Way, so in this case we are measuring the *total* line of sight extinction. We measured the strength of the Na I doublet using a combination of the two spectra obtained on December 7 and 10 (Section 3.3) to improve the signal-to-noise ratio to find EW(Na I D) = 1.32 Å. Applying the relation of Turatto et al. gives $E(B - V) = 0.21$ mag. However, there is considerable scatter in the relation of Turatto et al., typically on the order of ± 0.05 mag for EW(NaI D) ~1 Å. We can also measure the position of the centre of the Na I D absorption, which we find to be at 5907 Å. As this is approximately midway between the central wavelengths of this doublet for the Milky Way (rest) and host galaxy velocities, it seems likely that the internal extinction in the host is comparable to that in the foreground. From this, we would expect a total colour excess $E(B - V) = 0.05$ mag.

More qualitative measures of extinction involve comparing the colour and magnitude of the SN to similar objects; a comparison of the colour evolution of SN 2009md during the photospheric phase (Fig. 8), corrected for a colour excess $E(B - V) = 0.05$ mag, is a good match for the Type IIP SNe 1999em and 2005cs. We can also compare the colours and absolute magnitudes of nearby sources in pre-explosion images against the standard supergiant sequence of Drilling & Landolt (2000). We have taken the magnitudes of all sources found in *HST* WFPC2 pre-explosion images, within an arbitrary 3 arcsec radius of the progenitor, as discussed in Section 2.3, and plotted on a Hertzprung–Russell diagram in Fig. 4. We have also applied the selection criteria that sources must be found in both the $F606W$ and $F814W$ filters at a significance $\geq 5\,\sigma$, and must have χ^2 and sharpness statistics that are consistent with a non-extended source. The magnitudes of the sources in Fig. 4 have not been corrected for reddening, but only for the distance modulus. In addition, we plot a supergiant sequence from Drilling & Landolt with four differing amounts of reddening. As can be seen, the surrounding

[7] http://nedwww.ipac.caltech.edu/

Downloaded from https://academic.oup.com/mnras/article-abstract/417/2/1417/984687
by Leiden University user
on 23 November 2017

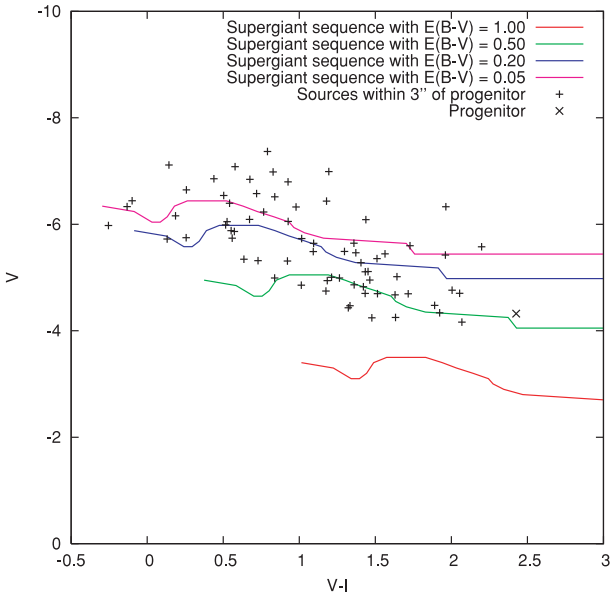

Figure 4. The absolute magnitude of all sources detected within 3 arcsec of SN 2009md, detected in archival *HST* WFPC2 *F*555*W* and *F*814*W* images at $\geq 5\sigma$, after applying sharpness and χ^2 cuts as discussed in text. The progenitor is marked with an 'x', nearby sources with a plus symbol; the progenitor appears to be very red, which supports its status as an evolved object. The coloured lines are a standard sequence of supergiants from Drilling & Landolt (2000), converted to Johnson–Cousins as per Bessel (1979), with different extinction values applied. The presence of blue sources seen close to the SN supports low levels of extinction; the best match appears to be for a colour excess of $E(B-V) \sim 0.05$–0.2 mag.

sources do not appear to be heavily reddened, the best match being with $E(B-V) = 0.2$ mag. It is important to remember, however, that at the distance of NGC 3389, 3 arcsec corresponds to ∼300 pc, and reddening can vary over such large scales.

Weaknesses can be identified in all the techniques used for estimating the reddening; low resolution spectra make it difficult to measure equivalent widths and line centres precisely; doubts have also been cast on the degree to which extinction and Na I correlate (Poznanski et al. 2011). Comparison of the local supergiant sequence is a crude test, at the distance to NGC 3389. Comparison of the colours of SN 2009md to those of other SNe is based on the assumption that these SNe are intrinsically similar. These caveats notwithstanding, we will adopt a value for $E(B-V) = 0.1^{+0.1}_{-0.05}$ mag. We also note that Fig. 4 provides support for the adopted distance to NGC 3389. From the arguments presented above, the reddening is not particularly high, and so in this case the fact that the identified sources do not appear to be systematically brighter or fainter than the supergiant sequence indicates that the distance we have adopted is correct.

2.6 Progenitor analysis: luminosity and mass estimates

In Smartt et al. (2009) the luminosities and temperatures of SN progenitors were calculated using *observationally* derived supergiant colours and bolometric corrections from the compilation of Drilling & Landolt (2000). However, the references from which Drilling & Landolt compiled their data are now over 40 years old, and so a re-evaluation and update of this methodology appear timely. In particular, Drilling & Landolt take their supergiant colours from Johnson (1966), where the magnitudes are in the photometric system of Johnson (1964). The *I* band defined by Johnson in these papers is substantially different from the modern Cousins *I* band which is used in the Johnson–Cousins system. Hence all $V-I$ colours in Drilling & Landolt (2000) should be converted from Johnson to Johnson–Cousins before use. A suitable transformation is given by Bessel (1979), which can be trivially applied to Drilling & Landolt.

However, we have chosen instead to use synthetic photometry of model spectra to define our bolometric corrections and colours, and hence derive a temperature and luminosity for the progenitor candidate (see e.g. Eldridge et al. 2007). Our reasons for doing so are several: by using synthetic photometry we can work in the *HST* filter system rather than having to convert to Johnson–Cousins filters, and we are not at risk of introducing errors due to the uncertain observed extinction towards red supergiants from the literature.

We have taken model spectra of massive red supergiants produced with the Model Atmospheres in Radiative and Convective Scheme (MARCS) code (Gustafsson et al. 2008) for a range of temperatures, and used the SYNPHOT package within IRAF to produce synthetic colours in the *HST* filter system, taking appropriate zero-points from Dolphin (2009). We have listed the derived *HST* filter system colours, together with the bolometric corrections from Levesque et al. (2005), for a range of model spectra at different temperatures in Table 1.

Taking the values for the progenitor magnitude from Section 2.3 together with the extinction and distance modulus as discussed in Sections 2.1 and 2.5, we calculate the progenitor absolute magnitude in the *HST* filter system to be $M_{F606W} = -5.18^{+0.38}_{-0.29}$, and the $F606W - F814W$ colour to be 1.74 ± 0.20. Using the values in Table 1 to determine the bolometric correction and temperature for this colour, we find a bolometric correction of -2.01 ± 0.3 mag for the progenitor of SN 2009md, and an effective temperature of 3530^{+70}_{-40} K, which according to Levesque et al. (2005) is consistent with a star of spectral type M4. Calculating the $F606W - V$ colour from Table 1 (which is essentially flat at -0.59 mag), and using this with the bolometric correction, we find a bolometric magnitude for the progenitor of $-6.60^{+0.43}_{-0.49}$ mag. We use the standard relation for luminosity and bolometric magnitude

$$\log L/L_\odot = \frac{M_{\rm bol} - 4.74}{-2.5} \quad (1)$$

to find a progenitor luminosity of $\log L/L_\odot = 4.54 \pm 0.19$ dex.

Table 1. Synthetic colours in the WFPC2 flight system from MARCS models and SYNPHOT.

$T_{\rm eff}$	$F450W - F555W$	$F555W - F606W$	$F606W - F814W$	$F555W - V$	BC
3400	1.288	0.633	2.307	0.044	−2.810
3500	1.416	0.616	1.852	0.029	−2.180
3600	1.475	0.602	1.543	0.019	−1.750
3700	1.476	0.583	1.341	0.015	−1.450
3800	1.442	0.560	1.203	0.016	−1.230
3900	1.391	0.536	1.105	0.019	−1.060
4000	1.336	0.511	1.030	0.024	−0.920

Downloaded from https://academic.oup.com/mnras/article-abstract/417/2/1417/984687
by Leiden University user
on 23 November 2017

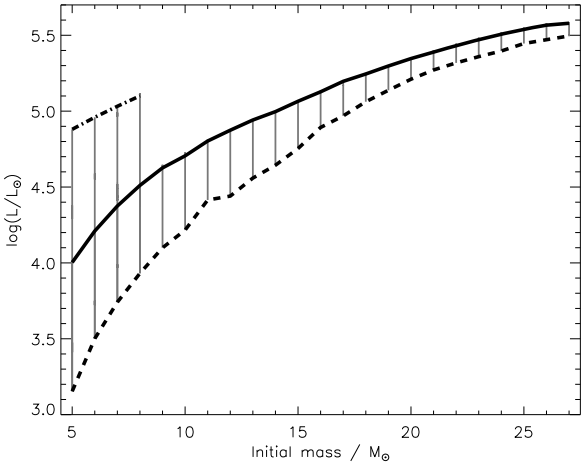

Figure 5. Luminosity as a function of mass from the STARS models. The solid line is the luminosity at model endpoint, or for models lower than 8 $M_\odot$, the pre-second dredge-up luminosity. The dot–dashed line is the progenitor luminosity after second dredge-up. The dashed line is the helium core luminosity of the model, from which the upper mass limit is obtained.

To use this luminosity to estimate a mass for the progenitor, it is necessary to compare to a series of evolutionary tracks. As discussed in Section 4.2, we have used the STARS models (Eldridge & Tout 2004) for comparison in this work. We find a best match for a pre-second dredge-up model of $8.5^{+6.5}_{-1.5}$ $M_\odot$, as shown in Fig. 5, although we stress that in this mass regime there are problems with stellar evolutionary models at later burning stages, which we will return to in Section 4.2. The upper limit for the mass is taken from the mass of the progenitor that would have a luminosity of 4.73 dex at the end of core He burning (for the reasons discussed in Smartt et al. 2009), which corresponds to 15 $M_\odot$, while the lower limit is found to be 7 $M_\odot$ from the uncertainty in the progenitor luminosity when plotted on the pre-second dredge-up track. The masses quoted here and in the rest of the paper refer to the zero-age main sequence mass of the progenitor, although for stars in this regime, mass loss over the lifetime of the star is quite low (0.6 $M_\odot$ for a 9 $M_\odot$ STARS model at solar metallicity).

For the non-detection in SOFI images, we have taken the bolometric corrections for the K_s filter from Levesque et al. (2005); these range from 3.16 to 2.33 mag for effective temperatures between ∼3200 K (early M type) and ∼4300 K (early K type), respectively. If we assume the effective temperature measured from the WFPC2 colours, the bolometric correction is closer to the former than the latter; however we will consider the two possibilities separately. For a cooler progenitor (and hence a larger bolometric correction), we find that the limiting luminosity log$L$ is 5.5 ± 0.1 $L_\odot$, with a corresponding upper mass limit of $M < 27$ $M_\odot$. For the hotter progenitor, we find a mass limit of $M < 36$ $M_\odot$. We have followed the maxim that it is better to err on the side of caution when presenting limits from non-detection, and so our final upper mass limits perhaps err on the conservative side.

2.7 Ruling out an SAGB progenitor and internal dust extinction

One factor that we have neglected up to this point is the possibility of circumstellar dust that is destroyed in the SN explosion. Several authors (e.g. Dwek 1983; Waxman & Draine 2000) have suggested that the initial X-ray and ultraviolet (UV) flash of an SN or gamma-ray burst could photoevaporate large quantities of dust in the vicinity of the progenitor. We would see no sign of this photoevaporated dust in the SN spectrum, and so there exists a possibility that we have underestimated the extinction towards the SN progenitor. Furthermore, red supergiants in the Galaxy and Magellanic Clouds are observed to suffer excess extinction when compared to nearby OB stars (Levesque et al. 2005; Massey et al. 2005), which has been interpreted as evidence for high levels of dust around these stars. Indeed, taking the sample of red supergiants from Levesque et al. (2005), we find a mean A_V of 0.7 mag. One caveat which must be attached to this, however, is that the extinction towards red supergiants will likely vary as a function of metallicity. Stars at a lower metallicity have a lower mass-loss rate, and so we may expect to find less circumstellar dust, and hence extinction. However, as we have adopted a solar metallicity (see Section 2.1), the comparison with Levesque et al. (2005) is appropriate.

To consider the impact of dust on our progenitor analysis, we recalculated the range of intrinsic progenitor colours and luminosities which are consistent with the observed progenitor $F606W$ filter magnitude and $F606W - F814W$ colour, leaving the extinction as a free parameter, as shown in Fig. 6. We have used the bolometric corrections for supergiants from Levesque et al.; these are likely appropriate for SAGB stars as well, as they are chiefly a function of colour (e.g. Drilling & Landolt 2000). We find that we can only produce a progenitor luminosity consistent with an SAGB star with $\gtrsim$2 mag of extinction in the V band. This level of reddening would mean that the progenitor is actually an early K supergiant, which is too hot to be an SAGB star, and so we can exclude an SAGB star as the progenitor for SN 2009md. In fact, it is quite difficult to make the progenitor more luminous by invoking dust – as the extinction is increased, the progenitor becomes intrinsically brighter in $F606W$, however to be self-consistent it must also be hotter, which implies a smaller bolometric correction. The two factors largely cancel each other out, leaving a progenitor of only marginally higher luminosity.

As can be seen in Fig. 6, we cannot exclude a higher mass, and hence more luminous, early K type red supergiant progenitor. However, we consider such a scenario unlikely. Taking the sample of red

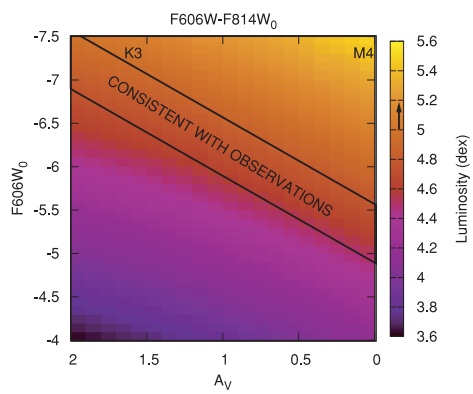

Figure 6. Progenitor luminosity as a function of extinction in the V-band and intrinsic $F606W$-filter absolute magnitude. On the lower x-axis is extinction in V, while the upper x-axis gives the corresponding intrinsic $F606W - F814W$ colour a progenitor would have with this degree of extinction, given that it has an apparent colour of $F606W - F814W = 1.84$ mag. On the y-axis is plotted the intrinsic progenitor magnitude in the $F606W$ filter. The bolometric luminosity, as indicated by the colour bar, has been calculated with equation (1), using appropriate bolometric corrections (from Levesque et al. 2005). Combinations of A_V and $F606W$ which are consistent with observations are marked. The black arrow on the colour bar indicates the typical SAGB luminosity that is expected to give rise to an electron-capture SN (Poelarends et al. 2008).

Downloaded from https://academic.oup.com/mnras/article-abstract/417/2/1417/984687
by Leiden University user
on 23 November 2017

Table 2. Magnitudes of local sequence stars used to calibrate the photometry of SN 2009md. Typical errors in magnitudes for sequence stars are $\lesssim 0.05$ mag.

Identifier	RA	Dec.	*U*	*B*	*V*	*R*	*I*
1	$10^h48^m28^s.1$	$12°32'25''$	19.544	18.573	17.677	17.043	16.579
2	$10^h48^m27^s.9$	$12°31'09''$	16.760	16.516	15.710	15.191	14.698
3	$10^h48^m33^s.7$	$12°31'35''$	20.621	20.621	19.340	18.351	17.313
4	$10^h48^m19^s.6$	$12°30'45''$	20.392	19.032	17.748	16.867	16.148
5	$10^h48^m21^s.6$	$12°33'47''$	17.536	17.341	16.757	16.351	16.028
6	$10^h48^m31^s.6$	$12°34'19''$	15.156	14.922	14.283	13.866	13.552

supergiants from Levesque et al. (2005), and selecting only those stars with both an observed V magnitude and a $V - I$ colour which are within 1 mag of that of the progenitor of SN 2009md, we find a mean A_V of 0.38 mag, with an rms scatter of 0.58 mag. Furthermore, only 12 per cent of the stars in this subset have a value of $A_V > 1$ mag, and only 4 per cent have $A_V > 1.5$ mag. We also note that, as expected, the heavily extinguished stars in the Levesque sample tend to have a redder colour than our progenitor candidate. An increase in A_V of ∼1 mag corresponds to an increase of ∼10 per cent in the initial mass as calculated in Section 2.6. This is smaller than our error bars and we thus conclude that it is unlikely that our results are affected by excess extinction.

3 FOLLOW-UP OBSERVATIONS

3.1 Photometric follow-up

A campaign of follow-up observations[8] was initiated for SN 2009md shortly after discovery, with data obtained from the Liverpool Telescope (LT) + RATCam and SupIRCam, the Faulkes Telescope North (FTN) + EM01, the NTT + EFOSC2 and SOFI, the NOT + ALFOSC, the Telescopio Nazionale Galileo (TNG) + NICS, the Calar Alto 2.2-m telescope + Calar Alto Faint Object Spectrograph (CAFOS), and the Wise Observatory Telescope + PI and Large Area Imager at Wise Observatory (LAIWO). The LT and FTN are identical 2-m robotic telescopes, located at Roque de los Muchachos, La Palma and Haleakala Observatory, Hawaii, respectively. Both telescopes have a standard pipeline that supplies reduced and calibrated images. For reduction of all other optical data, the QUBA[9] pipeline was used. The NTT + SOFI NIR data were reduced with the SOFI[10] pipeline and the TNG + NICS NIR data in IRAF using standard NIR reduction techniques.

All photometry was performed with the QUBA pipeline. Photometric zero-points and colour terms in the optical bands were determined for individual nights with aperture photometry of Landolt fields (Landolt 1992). Optical magnitudes for a sequence of stars in the SN field (Fig. 1) were then measured with PSF-fitting photometry. The final magnitudes of the local sequence stars were obtained averaging the measurements in five photometric nights. The coordinates and the average optical magnitudes of these stars are reported in Table 2. Corrected zero-points and colour terms for non-photometric nights were determined with reference to the average magnitudes in Table 3. NIR magnitudes for the local sequence stars were taken from the 2MASS catalogue (Skrutskie et al. 2006). The magnitudes of the SN at each epoch in the optical and NIR were measured with PSF fitting, and are listed in Tables 3 and 4.

In this and the following sections, we will chiefly compare SN 2009md to the sub-luminous Type IIP SN 2005cs (Pastorello et al. 2009). Our choice of comparison is motivated by the availability of photometry and spectra for this object, the detailed analysis in the literature and, most importantly, the fact that a progenitor was also identified for SN 2005cs. We will also make comparisons to SN 1999em as an example of a canonical Type IIP SN, and in some cases to the peculiar Type II SN 1987A as this is the best monitored and understood SN. Distances and reddening for SNe 2005cs, 1999em and 1987A were taken from Pastorello et al. (2009), Smartt et al. (2009) and Suntzeff & Bouchet (1990), respectively. The extinction as a function of wavelength for these SNe was calculated using the extinction law of Cardelli, Clayton & Mathis (1989).

Fig. 7 shows the evolution of SN 2009md in absolute magnitudes; the SN is clearly seen to be a Type IIP SN. The plateau phase of Type IIP SNe is governed by the release of the thermal explosion energy, and for SN 2009md lasts for ∼120 d. The magnitude of the SN is roughly constant during the plateau phase in the *I* band, but shows progressively larger rates of decline in bluer filters due to cooling and increased line blanketing. At the end of the plateau, when the thermal energy source created by the explosion is exhausted, the SN fades by ∼2.5 mag in ∼1 week. The tail phase that follows is governed by heating from the radioactive decay of ^{56}Co (the decay product of ^{56}Ni), making it possible to determine the ejected mass of ^{56}Ni. We will return to this issue in Section 3.2.

Fig. 8 shows the colour evolution of SN 2009md, as compared to SNe 1999em, 2005cs and 1987A. During the plateau phase we see a common colour evolution among the Type IIP SNe until the end of the plateau at ∼120 d. Beyond this phase, the colour evolution of all Type IIP SNe shows a trend towards redder colours due to the change in the temperature as the SN drops off the plateau. The colour change for SNe 2009md and 2005cs in this phase is more pronounced, as previously noted for sub-luminous Type IIP SNe (e.g. fig. 4 in Maguire et al. 2010b).

3.2 Bolometric light curve and ejected ^{56}Ni mass

The pseudo-bolometric *UBVRIJHK* light curves of SNe 2009md, 2005cs, 1999em and 1987A are shown in Fig. 9. The difference between these and a true bolometric light curve is caused by flux falling outside the covered wavelength range. At early times a substantial fraction of the flux is expected to fall in the UV. For SN 2005cs, Pastorello et al. (2009) showed that 60 per cent of the flux falls in the UV during the first ∼20 d, while it is negligible at late times. Assuming the Rayleigh–Jeans law the IR flux redwards of the *K* band is ∼5 per cent during the plateau phase and ∼10 per cent during the tail phase. Although we cannot exclude an IR excess we take

[8] This paper is based on ESO-NTT and TNG long-term programmes, in the framework of a large international collaboration for SN research. For the composition of the Collaboration and its scientific goals we refer the reader to our web pages (http://graspa.oapd.inaf.it/).

[9] IRAF-based Python package for photometry and spectroscopy developed by SV (Queens University Belfast). See Valenti et al. (2011) for details.

[10] ftp://ftp.eso.org/pub/dfs/pipelines/sofi

© 2011 The Authors, MNRAS **417,** 1417–1433
Monthly Notices of the Royal Astronomical Society © 2011 RAS

Downloaded from https://academic.oup.com/mnras/article-abstract/417/2/1417/984687
by Leiden University user
on 23 November 2017

Table 3. Log of optical photometric measurements of SN 2009md. Errors are given in parentheses.

JD-240 0000.5	Phase (d)	*U*	*B*	*V*	*R*	*I*	Instrument
55179.96	17.96		17.40 (0.07)	17.09 (0.05)	16.72 (0.15)		FTN (EM01)
55181.61	19.61		17.45 (0.12)	17.09 (0.09)	16.74 (0.05)	16.64 (0.03)	WISE (PI-CCD)
55182.02	20.02		17.54 (0.08)	17.07 (0.07)	16.72 (0.03)		FTN (EM01)
55183.96	21.96		17.60 (0.20)	17.05 (0.08)	16.72 (0.09)		FTN (EM01)
55189.83	27.83	18.42 (0.18)	17.73 (0.06)	17.11 (0.06)	16.72 (0.07)	16.55 (0.04)	NTT (EFOSC)
55189.96	27.96		17.87 (0.22)	17.16 (0.06)	16.76 (0.04)		FTN (EM01)
55192.00	30.00		17.92 (0.09)	17.17 (0.16)	16.77 (0.05)		FTN (EM01)
55192.60	30.60	18.73 (0.07)	17.94 (0.08)	17.20 (0.07)	16.78 (0.03)	16.70 (0.04)	LT (RATCam)
55194.09	32.09		17.98 (0.07)	17.17 (0.05)	16.76 (0.04)		FTN (EM01)
55197.55	35.55		18.05 (0.25)	17.21 (0.06)	16.82 (0.06)	16.59 (0.04)	LT (RATCam)
55202.72	40.72		18.17 (0.43)	17.28 (0.18)	16.82 (0.18)	16.60 (0.08)	CALTO (CAFOS)
55203.57	41.57			17.23 (0.05)	16.72 (0.06)	16.53 (0.04)	WISE (LAIWO)
55204.63	42.63	19.46 (0.36)	18.19 (0.39)	17.19 (0.07)	16.70 (0.08)	16.59 (0.04)	LT (RATCam)
55208.77	46.77	19.35 (0.21)	18.21 (0.18)	17.24 (0.13)	16.76 (0.06)	16.51 (0.04)	LT (RATCam)
55211.64	49.64	19.42 (0.11)	18.31 (0.04)	17.25 (0.15)	16.72 (0.08)	16.47 (0.03)	LT (RATCam)
55213.66	51.66	19.81 (0.31)	18.34 (0.12)	17.25 (0.10)			LT (RATCam)
55215.03	53.03		18.47 (0.27)	17.33 (0.18)	16.82 (0.10)	16.43 (0.25)	Mt. Ekar 1.82 m (AFOSC)
55219.74	57.74	19.89 (0.26)	18.42 (0.03)	17.30 (0.06)	16.77 (0.07)	16.46 (0.04)	NTT (EFOSC)
55224.51	62.51		18.50 (0.27)	17.34 (0.07)	16.78 (0.09)	16.55 (0.07)	LT (RATCam)
55232.45	70.45			17.42 (0.45)	16.78 (0.10)	16.51 (0.03)	LT (RATCam)
55233.47	71.47			17.39 (0.12)	16.80 (0.04)	16.52 (0.02)	LT (RATCam)
55233.65	71.65	20.10 (0.51)	18.68 (0.14)	17.39 (0.10)	16.86 (0.04)	16.51 (0.05)	NOT (ALFOSC)
55234.49	72.49			17.37 (0.17)	16.82 (0.10)	16.49 (0.06)	LT (RATCam)
55236.50	74.50			17.39 (0.12)	16.79 (0.06)	16.55 (0.02)	LT (RATCam)
55237.48	75.48		18.64 (0.15)	17.42 (0.07)	16.86 (0.03)	16.53 (0.05)	WISE (PI-CCD)
55238.52	76.52			17.42 (0.04)	16.83 (0.03)	16.53 (0.03)	LT (RATCam)
55245.81	83.81	20.49 (0.12)	18.81 (0.15)	17.52 (0.12)	16.90 (0.02)	16.53 (0.04)	NTT (EFOSC)
55246.47	84.47		18.86 (0.28)	17.45 (0.12)	16.90 (0.04)	16.60 (0.04)	WISE (INDEF)
55262.73	100.73	20.80 (0.25)	18.94 (0.04)	17.71 (0.04)	17.10 (0.03)	16.78 (0.04)	NTT (EFOSC)
55268.36	106.36			17.89 (0.05)	17.23 (0.04)	16.96 (0.04)	LT (RATCam)
55270.87	108.87		19.44 (0.58)	17.96 (0.17)	17.41 (0.20)	17.08 (0.15)	Mt. Ekar 1.82 m (AFOSC)
55274.48	112.48		19.58 (0.68)	18.07 (0.26)	17.43 (0.11)	17.14 (0.05)	WISE (PI-CCD)
55276.59	114.59	21.74 (0.54)	19.97 (0.15)	18.43 (0.16)	17.75 (0.06)	17.36 (0.05)	NOT (ALFOSC)
55277.44	115.44		20.13 (0.19)	18.51 (0.05)	17.80 (0.03)	17.46 (0.04)	LT (RATCam)
55278.47	116.47			18.73 (0.05)	17.96 (0.02)	17.60 (0.02)	LT (RATCam)
55279.51	117.51		20.58 (0.23)	18.96 (0.11)	18.16 (0.04)	17.73 (0.04)	LT (RATCam)
55280.54	118.54		20.98 (0.39)	19.26 (0.14)	18.40 (0.06)	17.97 (0.04)	LT (RATCam)
55282.38	120.38		21.45 (0.32)	20.07 (0.06)	18.98 (0.03)	18.51 (0.04)	LT (RATCam)
55285.61	123.61			20.51 (0.15)	19.14 (0.04)	18.71 (0.04)	LT (RATCam)
55288.41	126.41		22.54 (0.56)	20.53 (0.11)	19.35 (0.03)	18.70 (0.05)	NOT (ALFOSC)
55296.52	134.52		22.31 (0.28)	20.61 (0.12)	19.50 (0.08)		NOT (ALFOSC)
55314.48	152.48		22.64 (0.21)	20.81 (0.04)	19.68 (0.03)	19.02 (0.03)	NOT (ALFOSC)
55343.42	181.42			21.03 (0.06)	19.90 (0.03)	19.28 (0.04)	NOT (ALFOSC)
55349.43	187.43		22.82 (0.35)				NOT (ALFOSC)

Table 4. Log of infrared photometric measurements of SN 2009md. Errors are given in parentheses.

JD-240 0000	Phase (d)	*J*	*H*	*K*	Instrument
55209.58	47.58	16.11 (0.10)	15.85 (0.05)		LT (SupIRCam)
55220.73	58.73	16.13 (0.04)	15.82 (0.06)	15.70 (0.06)	NTT (SOFI)
55246.87	84.87	16.25 (0.03)	15.93 (0.07)	15.85 (0.07)	NTT (SOFI)
55263.60	101.60	16.51 (0.07)	16.14 (0.07)		NTT (SOFI)
55305.68	143.68	18.20 (0.06)	17.55 (0.11)	17.51 (0.11)	NTT (SOFI)
55348.41	186.41	18.53 (0.15)	17.89 (0.16)	17.92 (0.13)	TNG (NICS)
55352.88	190.88	>17.3	>16.0		LT (SupIRCam)

the last value as an estimate of the error in the pseudo-bolometric light curve during the tail phase.

To calculate the pseudo-bolometric light curves from the observed absolute magnitudes we interpolate the missing epochs in the filter light curves, and for each epoch integrate the total flux over the full wavelength range from *U* to *K*. To cover missing epochs in the filter light curves, we first linearly interpolated the magnitude for the filter with the most data. Missing data in successive neighbouring filters were then interpolated by adding/subtracting the linearly interpolated colour at that epoch. This scheme was used

Downloaded from https://academic.oup.com/mnras/article-abstract/417/2/1417/984687
by Leiden University user
on 23 November 2017

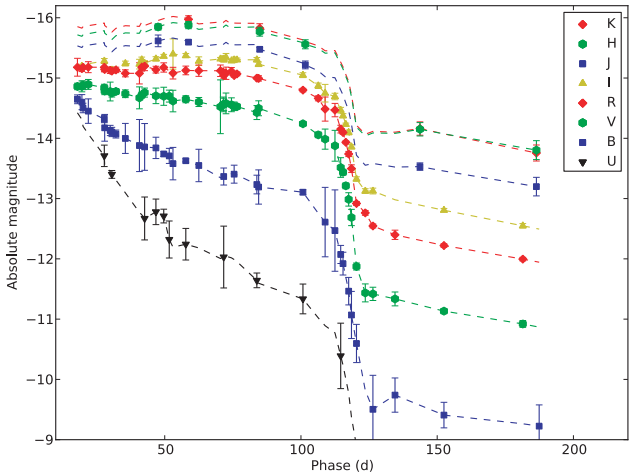

Figure 7. Full evolution of SN 2009md in *UBVRIJHK* filters. Solid points are the measured data points, while the dashed lines show the interpolated magnitudes used to compute the bolometric light curve.

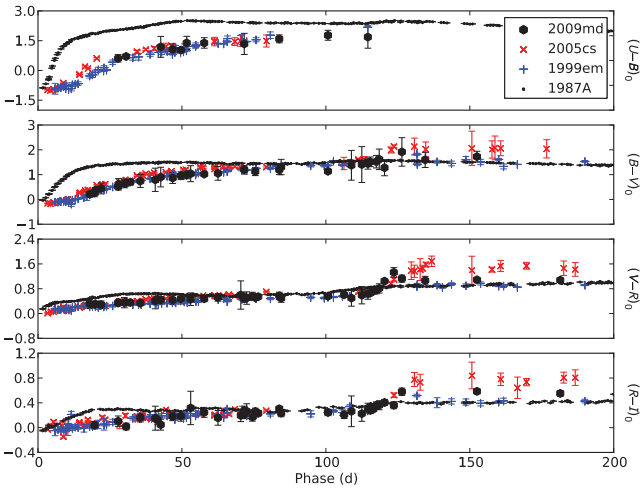

Figure 8. Colour evolution of SN 2009md, as compared to SNe 2005cs, 1999em and 1987A. The reddening at the end of the plateau for the sub-luminous Type IIP SNe is evident.

as the colour evolution of SNe is usually slower than the evolution in magnitude. NIR magnitudes are badly constrained at early times and during the drop off the plateau. The U-band magnitudes are also poorly constrained at very early and late times.

The total flux in the U to K wavelength range could then be calculated. We first loglinearly interpolated the flux per wavelength between the effective wavelengths of the filters. This was done under the constraint that the weighted average over the response functions (Moro & Munari 2000) equalled the flux per wavelength as determined by the zero-points (Bessel 1979; Cohen, Wheaton & Megeath 2003). The total flux was then integrated between the short and long wavelength half-maximum points of the U and K filters.

Comparing SN 2009md to SN 2005cs (Fig. 9), we see that they are indeed very similar, although the latter shows a sharper and deeper drop off the plateau. Comparing SNe 2009md and 2005cs to the normal Type IIP SN 1999em, we find that the plateau length is similar, but the plateau and tail luminosity are much lower. It is clear that SN 2009md, as far as the bolometric light curve is concerned, is a sub-luminous Type IIP SN.

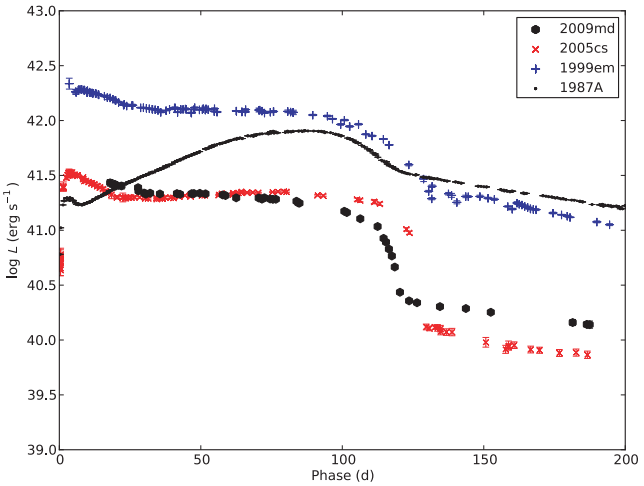

Figure 9. Pseudo-bolometric light curve for SN 2009md, integrated over the U to K wavelength range. For comparison, we show the sub-luminous Type IIP SN 2005cs, the normal Type IIP SN 1999em and the peculiar Type IIP SN 1987A.

We estimate the ^{56}Ni mass by comparing the pseudo-bolometric luminosity of SNe 2009md and 1987A (from the extensive Cerro Tololo Inter-American Observatory (CTIO) and South African Astronomical Observatory (SAAO) data sets). This assumes that the late-time ejecta are optically thick to the γ-rays produced by the ^{56}Co decay, and hence we are seeing all the luminosity from radioactive decay. This can be observationally tested by measuring the decline rate on the tail. The theoretically expected value for fully trapped γ-rays is 0.0098 mag d^{-1}. We measure the decline rate between 144 and 186 d to be 0.0082 ± 0.0017 mag d^{-1}, which is close but slightly lower than the theoretically expected value. A similar slow decline was also estimated for SN 2005cs. Pastorello et al. (2009) tentatively attributed it to the 'tail plateau phase' described by Utrobin (2007) caused by thermal radiation from the still hot inner ejecta. Comparing the pseudo-bolometric luminosities of SNe 2009md and 1987A at 186 d, and using a ^{56}Ni mass of 0.069 $M_{\odot}$ (Bouchet et al. 1991) for SN 1987A, we obtain an ejected ^{56}Ni mass for SN 2009md of $(5.4 \pm 1.3) \times 10^{-3}$ $M_{\odot}$.

3.3 Spectroscopic follow-up

Spectroscopic observations of SN 2009md were obtained with the NTT + EFOSC2 and SOFI, the Mt. Ekar 1.8-m telescope + Asiago Faint Object Spectrograph and Camera (AFOSC) and the NOT + ALFOSC. For all optical spectroscopic data, the QUBA pipeline was used to reduce the data in a standard manner. Most optical spectra were flux calibrated using spectroscopic standards obtained on the same night as the SN observations, but in a few cases such data were not available and archive sensitivity functions have been used instead. The NTT + SOFI NIR spectra were reduced with the SOFI pipeline, extracted with the TWODSPEC IRAF package and corrected for telluric absorption using a solar analogue spectroscopic standard and the known NIR spectrum of the Sun. Details of all spectroscopic observations, the telescope and instrument used, epoch and instrument characteristics are given in Table 5.

The optical spectral evolution from 12 to 142 d of SN 2009md is shown in Fig. 10, together with that of SN 2005cs (overplotted in red). It is clear from this figure and the detailed comparisons in Fig. 11 that SN 2009md is also spectroscopically very similar to

Downloaded from https://academic.oup.com/mnras/article-abstract/417/2/1417/984687
by Leiden University user
on 23 November 2017

Table 5. Log of spectroscopic observations of SN 2009md.

JD 240 0000	Phase (d)	Range (Å)	Resolution (Å)	Instrument
55173.78	12	3200–9100	21	NOT (ALFOSC)
55176.66	15	3200–9100	21	NOT (ALFOSC)
55189.27	27	3380–10320	16	NTT (EFOSC2)
55209.66	48	3200–9100	16	NOT (ALFOSC)
55216.08	54	3550–10000	25	Mt. Ekar 1.82-m (AFOSC)
55220.27	58	9500–16400	22	NTT (SOFI)
55245.28	83	3380–10320	16	NTT (EFOSC2)
55262.17	100	3380–10320	16	NTT (EFOSC2)
55263.16	101	9500–16400	22	NTT (SOFI)
55263.21	101	15300–25200	34	NTT (SOFI)
55271.97	110	3550–10000	25	Mt. Ekar 1.82-m (AFOSC)
55304.17	142	3685–9315	21	NTT (EFOSC2)

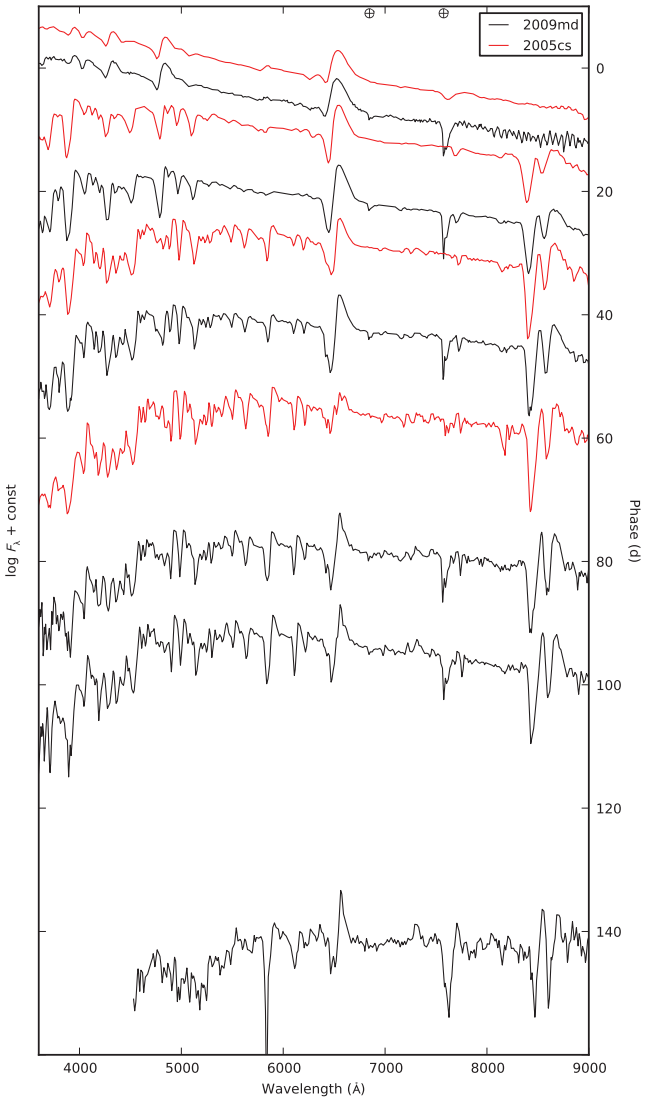

Figure 10. Time series of spectra for SNe 2009md (black) and 2005cs (red). To visualize the temporal evolution the spectra have been aligned to the time axis at the right border of the panel. The spectra have been corrected for redshift and dereddened. Telluric features are indicated with a ⊕ symbol. The lower signal-to-noise ratio spectra of SN 2009md from the Mt. Ekar 1.82-m telescope and at 15 d from NOT have been excluded for clarity.

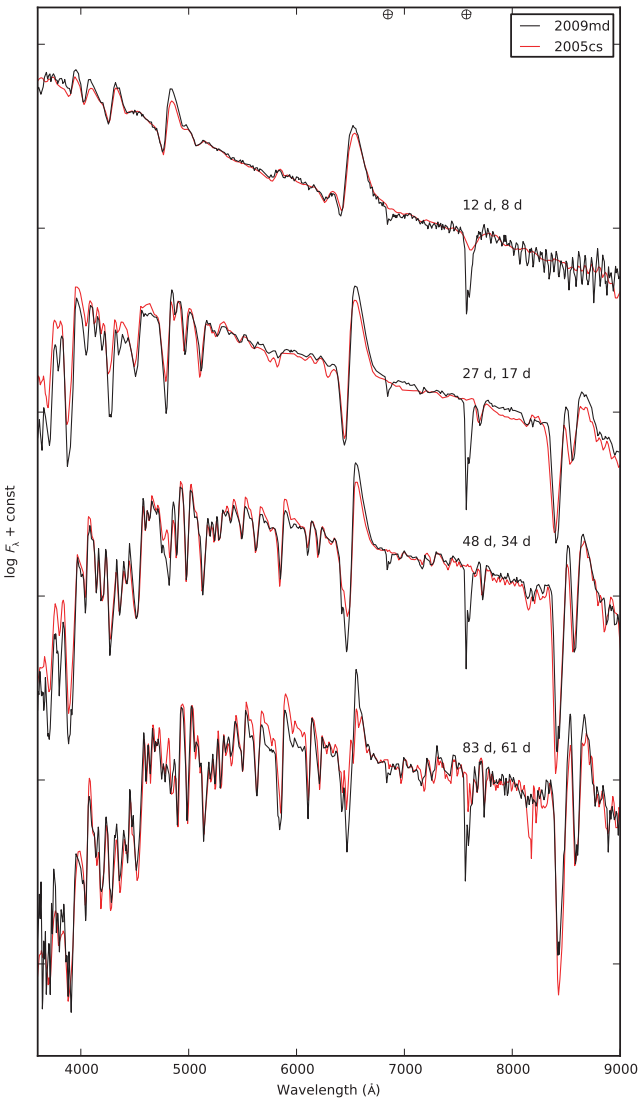

Figure 11. Overplots of the epochs shown in Fig. 10 giving the best match in Supernova Identification (SNID) (Blondin & Tonry 2007). The spectra have been corrected for redshift and dereddened. Telluric features are indicated with a ⊕ symbol.

Downloaded from https://academic.oup.com/mnras/article-abstract/417/2/1417/984687
by Leiden University user
on 23 November 2017

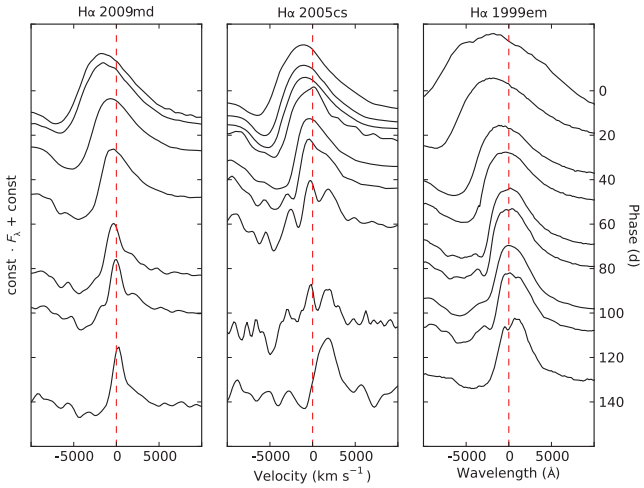

Figure 12. Time evolution of the Hα line in SN 2009md (left-hand panel), as compared to SNe 2005cs (centre panel) and 1999em (right-hand panel). To visualize the temporal evolution the spectra have been aligned to the time axis at the right border of each panel. The spectra have been corrected for redshift and dereddened. The emission peak is noticeably blueshifted at earlier epochs.

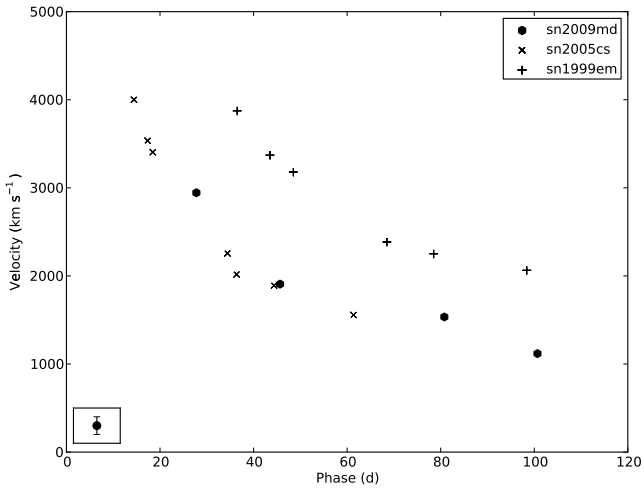

Figure 13. Photospheric velocity evolution of SN 2009md as measured from the Sc II 6246 Å line, compared to those of SNe 2005cs and 1999em. The typical measurement error is indicated in the lower-left corner.

SN 2005cs. The spectral evolution very much follows that of SN 2005cs as described in Pastorello et al. (2009). At early epochs, the spectrum has a blue continuum, with the dominant features being H and He lines together with some evidence of Si II and Fe II. Around 10–30 d post explosion, the O I λ7774, Ca II H & K lines and NIR triplet, Na I D and numerous strong Fe II lines appear. At later times the continuum becomes redder and a number of other metal lines appear, such as Ti II, Sc II and Ba II, and absorption features grow deeper. As the linewidths in sub-luminous Type IIP SNe are smaller than in normal Type IIP SNe, lines that are normally blended may be resolved. This may explain the Ba II line which appears in the blue wing of the Hα line and other features not seen in normal Type IIP SNe spectra.

Despite the similarity to SN 2005cs there are also some noticeable differences. In Fig. 12 we show the evolution of the Hα line as compared to SNe 2005cs and 1999em. It can be seen that the Hα evolution between 60 and 120 d is rather different, with the line appearing weaker at later epochs in SN 2005cs as compared to SN 2009md. Comparing the time series of spectra of SN 2009md with SN 2005cs in Fig. 10, the former appears to be evolving more slowly than the latter; this is also confirmed by cross-correlation of the spectra using SNID (Blondin & Tonry 2007). At ∼10 d the match is quite good, at 27 d the best match is 17 d, at 48 d the best match is 34 d, and at 83 d the best match is 61 d, where the former epochs refer to SN 2009md and the latter to SN 2005cs.

In Fig. 13, the velocity evolution of the Sc II λ6246 line as measured from the P-Cygni minimum is shown. This line is believed to be a good indicator of the photospheric velocity (Maguire et al. 2010a). As seen in Fig. 13 the line velocities are considerably lower for SNe 2009md and 2005cs than for the normal Type IIP SN 1999em. We have already shown that SN 2009md satisfies two of the criteria of the sub-luminous Type IIP SNe, namely a faint absolute magnitude, and a low ejected ^{56}Ni mass. As low line velocities are the third signature we can thus classify SN 2009md as a sub-luminous Type IIP SN.

Two epochs of NIR spectra of SN 2009md were obtained with NTT + SOFI, the first at 58 d and the second at 101 d (Fig. 14). Ideally, we would compare these to the same SN as in the optical at a similar epoch; unfortunately the dearth of NIR spectra precludes this. Hence we have compared the 58 d spectrum to SN 2005cs and the 101 d spectrum to SN 1997D.

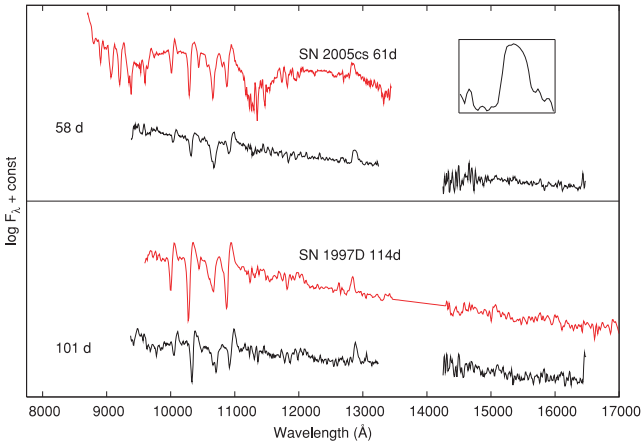

Figure 14. De-reddened and redshift-corrected NIR spectra of SN 2009md. The upper panel shows SN 2009md (in black) at the midpoint of the plateau phase, as compared to SN 2005cs at a similar epoch. The second panel shows SN 2009md at the end of the plateau, as compared to the sub-luminous SN 1997D. The box in the upper panel shows a magnified view of the shape of the Paβ line at 58 d as discussed in the text.

At 58 d, the NIR spectrum of SN 2009md displays the series of Paschen lines from H. Paβ at 1.28 μm appears only in emission, and appears to have a somewhat boxy profile. Boxy line profiles are usually associated with an optically thin line (e.g. Fransson 1984). It is hence possible that the Paβ emission we observe is formed further out in the ejecta. Paγ and Paδ at 1.09 and 1.00 μm, respectively, have P-Cygni profiles. The Paγ line is blended with He I at 1.083 μm.

4 DISCUSSION

In the following, we use the standard candle method for Type IIP SNe to verify the distance to NGC 3389. We attempt to explain the discrepancy between the predictions of stellar evolutionary models and the observed luminosity of sub-luminous Type IIP SN

Downloaded from https://academic.oup.com/mnras/article-abstract/417/2/1417/984687
by Leiden University user
on 23 November 2017

progenitors. The mass range of progenitors which produce sub-luminous Type IIP SNe is estimated from both progenitor detections and SN rates. We also discuss the relationship of the ejected ^{56}Ni mass to the progenitor luminosity.

4.1 Verifying the distance to SN 2009md

To verify the distance to the host galaxy of SN 2009md, NGC 3389, we use the standard candle method for Type IIP SNe (Hamuy & Pinto 2002; Poznanski et al. 2009; D'Andrea et al. 2010). Hamuy & Pinto (2002) show that the V-band magnitude and expansion velocity of Type IIP SNe satisfy the equation

$$V_{\rm p} - A_V + 6.504(\pm 0.995)\log\left(\frac{v_{\rm p}}{5000}\right) = 5\log(cz) - 1.294(\pm 0.131), \quad (2)$$

where $V_{\rm p}$ is the apparent V-band magnitude at 50 d post explosion, $v_{\rm p}$ is the expansion velocity in km s^{-1} at the same epoch, A_V is the V-band extinction in magnitudes and z is the redshift of the host galaxy. Taking the magnitude of SN 2009md at 50 d from Table 3, $V_{\rm p} = 17.30 \pm 0.03$ mag, and the expansion velocity of ~2000 km s^{-1} from the spectrum of SN 2009md closest to 50 d (Fig. 13), we find a host galaxy redshift $z = 0.0046$, corresponding to a distance modulus of 31.38 mag. This is in good agreement with the distance estimates presented in Section 1.

Maguire et al. (2010a) have extended the technique to the NIR, where they find a trend of reduced dispersion compared to optical wavelengths in the resultant Hubble diagram. Modifying equation (1) of Maguire et al. to solve for the distance modulus

$$\mu = m_J - J_0 + \alpha\log_{10}\frac{v_{\rm Fe\,II}}{5000} - R_J[A_V - A_J] \quad (3)$$

and using the Sc II velocity of 2000 km s^{-1} and $m_J = 16.112 \pm 0.097$ mag from the spectrum and NIR photometry at ~ 50 d, together with the values of $J_0 = -18.06 \pm 0.25$ mag, $R_J = 0.108$ and $\alpha = 6.33 \pm 1.2$ (where α is a fitting constant) from Maguire et al., we obtain a distance modulus $\mu = 31.63 \pm 0.55$ mag, which again is in agreement with the distance presented in Section 1, $\mu = 31.64 \pm 0.21$.

4.2 Producing faint progenitors with evolutionary models

The classical picture of stellar evolution sees stars with a main-sequence mass $\lesssim 8$ M$_\odot$ form white dwarfs, stars with $8 \lesssim M \lesssim 11$ M$_\odot$ become SAGB stars which may lead to electron-capture SNe (ECSNe), and stars with $M \gtrsim 11$ M$_\odot$ burning through to iron core collapse (see e.g. Woosley, Heger & Weaver 2002). Unfortunately, the mass range over which these changes occur is small (and indeed comparable to the uncertainty in our progenitor mass). Furthermore, the precise mass thresholds for each of the three regimes are sensitive to the details of the evolutionary models used, with the most uncertain aspects of stellar evolution, namely convection and mixing, nuclear reaction rates, and the neutrino cooling rate, being most significant for this regime. In recent years, however, there have been several detections of low-luminosity progenitors, which lead us to question the accuracy of this picture (Smartt et al. 2009).

There is a lack of stellar evolutionary models which follow stars at the low end of the mass range of Type IIP progenitors through, and beyond, core helium burning. This is significant as there are differences between the various codes, in terms of not only the numerical techniques used, but also their treatment of some of the more uncertain physics in the models, e.g. mixing related phenomena such as rotation and convective overshooting. To examine the differences between some of the available codes, we took a 9 M$_\odot$ model at solar metallicity ($Z = 0.020$), and examined its luminosity at the end of core He burning (which we have defined as when the core He fraction by mass drops below 1 per cent). We have plotted the luminosity against temperature for the rotating Geneva (Meynet & Maeder 2003), STARS (Eldridge & Tout 2004) and Siess (2006) codes in Fig. 15. All three codes are in agreement to within 0.1 dex in the luminosity at the end of core He burning. On the basis of this, we can conclude that while there exists a need for models that follow stellar evolution to later stages, the problems discussed in the following are not model-specific, and can instead be attributed to a more general problem with our understanding of stars in this mass range.

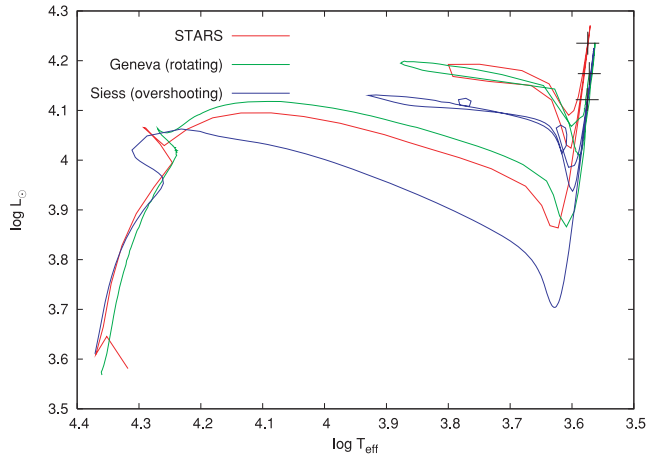

Figure 15. Comparison of evolutionary codes at the end of core He burning (the last stage all three codes are evolved through). All models are for a star with an initial mass of 9 M$_\odot$, at solar metallicity. The point of core He exhaustion is marked for all three tracks with a '+' symbol.

AGB and SAGB stars arise after several dredge-ups in between the major nuclear burning stages of stellar evolution. After the star forms an He core, it will ascend the red giant branch. This is accompanied by a deepening of the stars convective envelope that mixes nuclear processed material to the surface of the star during the first dredge-up. This process terminates with the ignition of core He burning. The process occurs again at the end of core He burning, in a second dredge-up. As before, a deep convective envelope penetrates into the star, and brings the majority of the He which surrounds the carbon–oxygen (CO) core to the surface. The star is then left with a CO core, essentially a CO white dwarf, surrounded by thin He- and H-burning shells. Such an arrangement is unstable, and so burning progresses in a series of thermal pulses (e.g. Stancliffe, Tout & Puls 2004). In the most massive cases the CO core is massive enough that carbon is ignited and the CO core is processed into an oxygen–neon (ONe) core. Such a star is called a Super-AGB star. If the ONe core reaches the Chandrasakhar mass, then an electron capture core collapse will occur (Eldridge & Tout 2004; Siess 2007; Poelarends et al. 2008; Pumo et al. 2009).

The fact that the progenitor identified for SN 2009md has a luminosity of ~4.54 dex indicates that this star has not undergone the second dredge-up, and hence is not an SAGB star. Furthermore, there have now been several detections of progenitors with similarly low luminosities (e.g. SNe 2005cs, 2003gd & 2008bk). The problem of the low luminosities has been discussed by Smartt et al. (2009); for a full discussion of the issues raised the reader is referred to this work.

Downloaded from https://academic.oup.com/mnras/article-abstract/417/2/1417/984687
by Leiden University user
on 23 November 2017

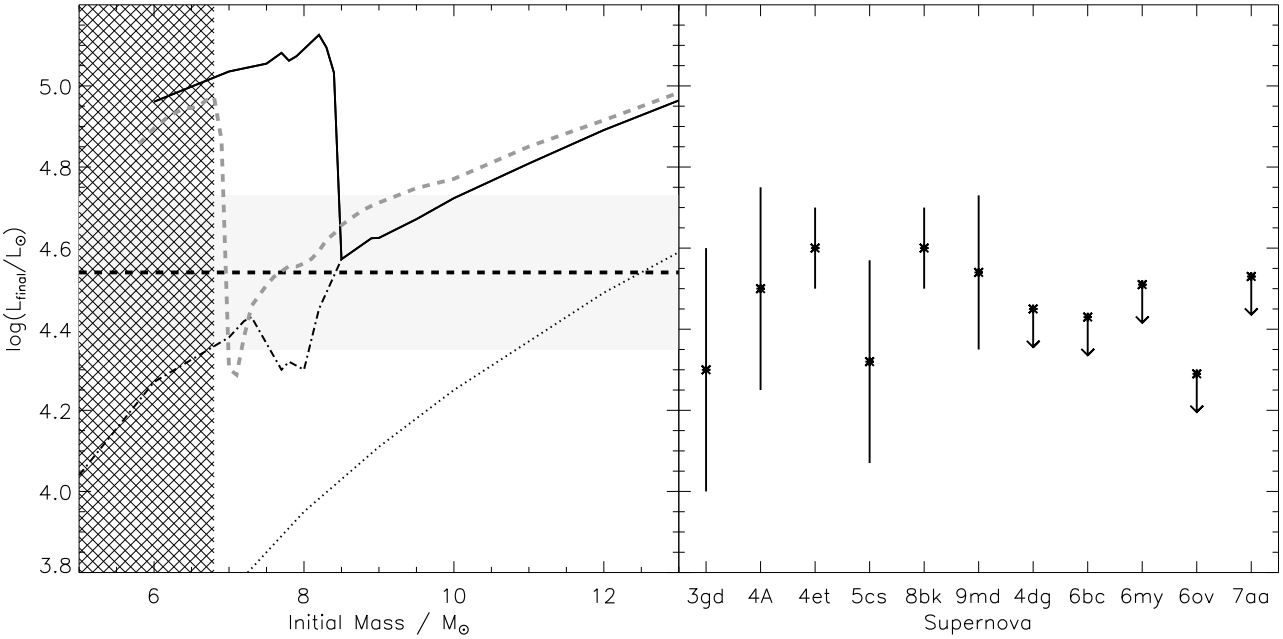

Figure 16. The luminosity of models as a function of mass, similar to Fig. 5, but showing the effects of enhanced carbon burning. In the left-hand panel, the solid black line is the final luminosity of the standard STARS model, and the dashed grey line is the final luminosity of the STARS model with an enhanced ^{12}C burning rate. The dash–dotted line is the luminosity of the standard STARS models immediately prior to second dredge-up, and the dotted line is the standard model luminosity at the end of core helium burning (which is the same for both normal and enhanced carbon burning models). We indicate the region in which stars will not explode as core-collapse SNe with a hatched area. In the right-hand panel, we show progenitor luminosities from detections and upper limits.

To explain the fact that we now have several SNe where the progenitor is less luminous than expected from evolutionary models, we are left with two possibilities: either prevent the second dredge-up from occurring, or ensure that the star evolves rapidly enough that it explodes before the second dredge-up. The former option is more difficult. Although convection-related phenomena are some of the least well-understood aspects of stellar evolution models, it is difficult to find a physical process that will prevent convection in and around the core and thus prevent second dredge up. We thus turn to attempting to force stellar evolution to proceed faster. The one key detail that may be most uncertain in current models is the carbon-burning rate. Recent measurements of the ^{12}C cross-section suggest that a resonance may be present that boosts the burning rate by a factor of 10^5 (Spillane et al. 2008). To investigate the effect of this new higher rate, we have created a series of stellar models similar to those discussed in Eldridge & Tout (2004) with the carbon-burning rate boosted by such a factor. We find that the increase in the ^{12}C burning rate decreases the minimum mass for an SN by one solar mass to 7 $M_\odot$ but except for a narrow mass range, the final luminosity of the models does not decrease, and so the problem remains (see Fig. 16).

It is difficult to follow these models with enhanced carbon burning though to the formation of an iron core, as the formation of a very hot, thin shell around the degenerate core causes numerical difficulties. However, the high temperatures reached in the core towards the end of the models ($10^{9.3}$ K) suggests that these models may in fact form an Fe core. This is helped by the avoidance of the second dredge-up, as the core does not become dense enough for significant cooling through neutrino emission before the latter burning stages. However, we must once again stress that this is an exploratory *attempt* to produce a model which avoids second dredge-up, and may, or may not, be correct.

4.3 The mass range of the progenitors of sub-luminous Type IIP SNe

If we assume two channels for sub-luminous Type IIP SNe, a 'low-mass' channel between an arbitrary mass range of 8–10 $M_\odot$ and a 'high-mass' channel between an arbitrary mass range of 23–27 $M_\odot$, then for a standard Salpeter initial mass function (IMF) with a slope of -2.35, $\sim$5 times as many sub-luminous SNe will come from the low-mass channel as from the high-mass channel. In this context, the fact that the three detected sub-luminous SN progenitors (for SNe 2008bk, 2005cs and 2009md) are all low mass is not surprising.

While we can clearly say from the progenitors of sub-luminous Type IIP SNe found so far that at least a significant fraction of them come from low-mass progenitors, as shown in Fig. 17, it is of interest to try and restate this in more quantitative terms. Hence, we have followed the methodology of Smartt et al. (2009) in calculating the probable maximum and minimum mass for Type IIP core-collapse SNe (for a detailed description of the methodology the reader is referred to this paper). In brief, we have two free parameters, $M_{\rm min}$ and $M_{\rm max}$, which are the minimum and maximum masses for SN progenitors, respectively. We calculate the likelihood of a progenitor having a mass with respect to the IMF, maximizing this over all progenitors and upper limits. An important point to note is that only *detections* are taken into account when calculating the lower mass limit; this is because the non-detections of progenitors leave the lower mass unconstrained, and due to the nature of the IMF, these will tend towards lower masses. We are also assuming that sub-luminous Type IIP SNe come exclusively from a single continuous mass range.

We have three progenitor detections, and two upper limits on mass. To ensure a consistent approach, we have recalculated the progenitor masses of SNe 2005cs, 2008bk, 2005ov and 1999br

Downloaded from https://academic.oup.com/mnras/article-abstract/417/2/1417/984687
by Leiden University user
on 23 November 2017

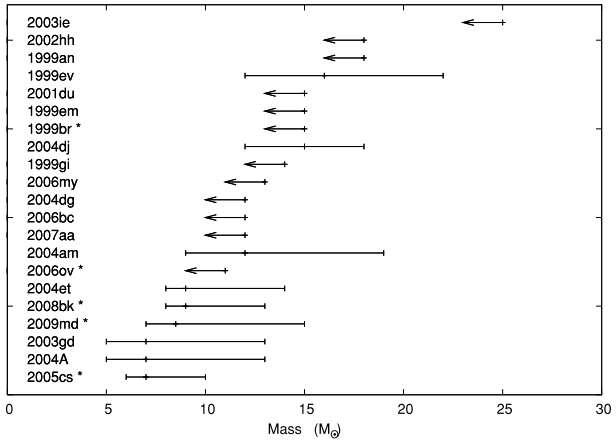

Figure 17. Measured masses for the sample of SNe from Smartt et al. (2009) with progenitor detections or upper mass limits. SN 2009md is also added to this figure. Sub-luminous Type IIP SNe are marked with an asterisk, and have had their masses or mass limits recalculated using synthetic photometry of MARCS models as discussed previously.

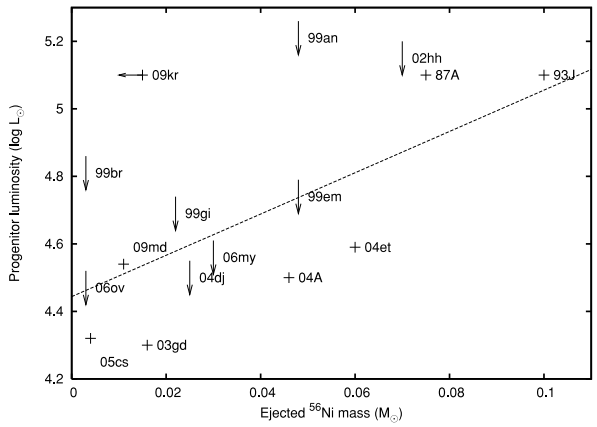

Figure 18. Ejected ^{56}Ni mass against progenitor luminosity (plus symbol) or luminosity limit (arrow), for the sample of Type IIP SNe with both measured progenitor luminosities or limits, and Ni^{56} masses. A least-squares fit to the measured masses is also shown with a dashed line.

using the synthetic photometry approach discussed in Section 2.6. We find that the upper limit for the progenitor of SN 1999br is unchanged at <15 M$_\odot$, SN 2006ov increases by <11 M$_\odot$, and the progenitor masses of SNe 2005cs and 2008bk remain the same (although the uncertainty in the mass of the former is increased). We calculate the most probable progenitor mass range for the sub-luminous Type IIP SNe to be between 7.5 and 9.5 M$_\odot$, although as this is based on so few data points the significance of this result is low.

As a consistency check, taking all SNe in the volume and time limited sample of Smartt et al. (2009) (within 20 Mpc, discovered between 1998 January and 2008 June) we can calculate the relative rate of sub-luminous SNe as a fraction of all Type IIP SNe to be 23 per cent. Using this, and assuming upper and lower mass limits for Type IIP SN progenitors of 8.5 and 16.5 M$_\odot$ respectively (Smartt et al. 2009) and a Salpeter IMF, we find the maximum mass for a sub-luminous Type IIP progenitor to be 9.3 M$_\odot$ which is in accordance with that the mass range suggested previously.

4.4 Explosion energy and ejecta mass

Using simple scalings, we can compare the explosion energy E and ejecta mass M of SN 2009md to those of SN 1999em. Equations (1) and (2) in Kasen & Woosley (2009) give scalings for E and M in terms of the plateau luminosity $L_{\rm sn}$, duration $t_{\rm sn}$, ejecta velocity $v_{\rm sn}$ and progenitor radius R,

$$E \propto \frac{L_{\rm sn} t_{\rm sn}^2 v_{\rm sn}}{R} \tag{4}$$

$$M \propto \frac{L_{\rm sn} t_{\rm sn}^2}{R v_{\rm sn}}. \tag{5}$$

From Fig. 9 we see that the plateau lengths are similar, while the plateau luminosity is a factor of ∼7 lower for SN 2009md. From Fig. 13 we see that the ejecta velocity is ∼1.5 lower for SN 2009md. The radius of SN 2009md is estimated to be ∼500 R$_\odot$ from the effective temperature and luminosity given in Section 2.6, which is comparable to the value found for SN 1999em by Utrobin (2007). This gives a factor of ∼10 lower energy and a factor of ∼5 lower mass. Although a crude estimate, this clearly suggests a very low explosion energy and a low ejecta mass as compared to normal Type IIP SNe.

4.5 The production of ^{56}Ni

The ^{56}Ni synthesized in SNe, which powers the late-time luminosity after the plateau stage, is largely formed by the explosive burning of oxygen and silicon. As noted by Eldridge et al. (2007) and Kitaura et al. (2006), an SAGB progenitor will have little oxygen and silicon surrounding the core, and hence we may expect a SAGB star to produce a low mass of ejected ^{56}Ni. But a low-mass (∼9 M$_\odot$) progenitor of an Fe core-collapse SN will also produce a small quantity of ejected ^{56}Ni for the same reason. A high-mass (∼25 M$_\odot$) progenitor can also lead to the apparent formation of small quantities of ^{56}Ni, as the ^{56}Ni that is synthesized falls back on to the nascent black hole (e.g. Woosley & Weaver 1995; Heger et al. 2003).

The low mass of ejected ^{56}Ni seen in SN 2009md is extremely low when compared to that of a normal Type IIP, albeit twice as high as the 3×10^{-3} M$_\odot$ ^{56}Ni mass estimated for SN 2005cs by Pastorello et al. (2009).

We have plotted the ejected ^{56}Ni mass against progenitor luminosity for a sample of SNe in Fig. 18. The degree to which ^{56}Ni mass and progenitor luminosity correlate is striking, although given that the ejected nickel mass is dependent on the final core mass, and the final core mass will be dependent on the initial mass of the star and hence linked to luminosity, perhaps not so surprising. Even the peculiar Type IIP SN 1987A, and SN 1993J, for which a binary scenario was proposed, follows the relation well.

5 CONCLUSIONS

To understand SNe and their progenitors, it is necessary to take a holistic approach, and draw together observational data on both the progenitor and its explosion, together with the theoretical framework to interpret these data.

We find a faint, red source in archival images coincident with SN 2009md. We find a best match to a low-mass red supergiant, with $M = 8.5^{+6.5}_{-1.5}$ M$_\odot$, and favour this as the progenitor. While there is some uncertainty as to how the final stages of low-mass SN progenitors evolve (as discussed in Section 4.2), we can be confident that neither a SAGB star nor a high-mass star is the progenitor of SN

Downloaded from https://academic.oup.com/mnras/article-abstract/417/2/1417/984687
by Leiden University user
on 23 November 2017

2009md. We have made some tentative attempts to evolve a series of low-mass models using the STARS code to match our observations, and find that by boosting the carbon burning rate we can alter the final luminosity of models, and lower the minimum mass for the models to not undergo second dredge-up. We stress, however, that this is only a first attempt, and that there is a need to both evolve the codes closer to core collapse, and to establish whether the enhanced C burning we suggest actually occurs.

This is the third direct detection of the progenitor of a sub-luminous Type IIP, confirming that at least a significant fraction of this class of SNe comes from low-mass ($\sim$8 $M_{\odot}$) stars. It is tempting to suggest a scenario in which all these SNe come from low-mass progenitors, and are produced by low-energy Fe core-collapse explosions which eject small amounts of ^{56}Ni. However, we cannot rule out the presence of a population of high-mass fallback SNe, although we can confirm that if such a population does exist, we have yet to observe its progenitors.

The evolution of SN 2009md is remarkably similar to that of the sub-luminous Type IIP SN 2005cs, with the main difference being the apparently faster spectroscopic evolution of the latter. In terms of absolute magnitude and line velocities, however, we can regard SN 2009md as SN 2005cs's twin.

In this paper, we have presented data from the first $\sim$6 months of SN 2009md. In many ways though, the most interesting work remains to be done. We have presented a challenge, to model an SN progenitor with a low luminosity immediately prior to core collapse. Such a challenge is far from simple, as the ever more rapid burning of successively heavier elements, combined with dynamical processes such as convection and dredge-up, conspires to make the final years of a star's life the hardest to model. We have also presented a challenge to attempt to model the explosion of a low-mass star with an Fe core. If our suggestion that the core of low-mass progenitors may in fact become hot enough to burn through to Fe (based on our enhanced C burning models) is correct, then it is of great interest to model an Fe core collapse in a low-mass star.

Observationally, there is also future work to be done. Some years hence, deep images of the site of SN 2009md with either an 8 m class telescope, the *HST* or (future) *James Webb Space Telescope* can confirm the disappearance of the progenitor (e.g. Maund & Smartt 2009; Gal & Leonard 2009). Accurate measurements of any remaining flux at the progenitor coordinates may also reduce the uncertainties in progenitor mass and luminosity. Another interesting, but less direct, test of the progenitor scenario we have proposed for SN 2009md may be to measure the oxygen abundances in late time nebular spectra. Kitaura et al. (2006) propose such a test to distinguish between low- and high-mass progenitors, as the former should eject considerably less oxygen (perhaps one hundredth to one thousandth of the mass).

ACKNOWLEDGMENTS

MF is funded by the Northern Ireland Department of Employment and Learning. This work was conducted as part of a European Young Investigator (EURYI) scheme award (esf.org/euryi). The Oskar Klein Centre (ME, JS) is funded by the Swedish Natural Science Research Council. SB, FB and MT are partially supported by the Progetto Di Ricerca Di Interesse Nazionale-Istituto Nazionale Di Astrofisica (PRIN-INAF) 2009 with the project 'Supernovae Variety and Nucleosynthesis Yields'. The Dark Cosmology Centre is funded by the Danish National Research Foundation. AG's work is supported by grants from the Israeli Science Foundation, an FP7 Marie Curie IRG fellowship, a research grant from the Peter and Patricia Gruber Awards, the Weizmann-Minerva program and the Benoziyo Center for Astrophysics.

Based on observations obtained at the Gemini Observatory (GN-2010A-Q-54, PI: Crockett & Gal-Yam), which is operated by the Association of Universities for Research in Astronomy, Inc., under a cooperative agreement with the NSF on behalf of the Gemini partnership: the National Science Foundation (United States), the Science and Technology Facilities Council (United Kingdom), the National Research Council (Canada), CONICYT (Chile), the Australian Research Council (Australia), Ministrio da Cincia e Tecnologia (Brazil) and Ministerio de Ciencia, Tecnologa e Innovacin Productiva (Argentina). Based on observations made with the NASA/ESA *HST*, obtained from the data archive at the Space Telescope Institute. STScI is operated by the association of Universities for Research in Astronomy, Inc. under the NASA contract NAS 5-26555.

Based on data collected at the CFHT. Based on observations made with the NOT, operated on the island of La Palma jointly by Denmark, Finland, Iceland, Norway and Sweden, in the Spanish Observatorio del Roque de los Muchachos of the Instituto de Astrofisica de Canarias. Partially based on observations made with the Italian TNG operated on the island of La Palma by the Fundacin Galileo Galilei of the INAF (Istituto Nazionale di Astrofisica) at the Spanish Observatorio del Roque de los Muchachos of the Instituto de Astrofisica de Canarias. The LT is operated on the island of La Palma by Liverpool John Moores University in the Spanish Observatorio del Roque de los Muchachos of the Instituto de Astrofisica de Canarias with financial support from the UK Science and Technology Facilities Council. The FTN is operated by the Las Cumbres Observatory Global Telescope Network (Hawaii). Based on observations collected at the European Organisation for Astronomical Research in the Southern Hemisphere, Chile (Proposal 184.D-1140). LAIWO, a wide-angle camera operating on the 1-m telescope at the Wise Observatory, Israel, was built at the Max Planck Institute for Astronomy (MPIA) in Heidelberg, Germany, with financial support from the MPIA, and grants from the German Israeli Science Foundation for Research and Development, and from the Israel Science Foundation. Partially based on observations collected at Asiago observatory and Calar Alto Observatory. We especially thank the support staff and telescope operators involved in these observations for their skill, assistance and advice.

This work has been greatly facilitated and expedited by the European supernova collaboration involved in ESO-NTT large program 184.D-1140 led by Stefano Benetti.

This research has made use of the NASA/IPAC Extragalactic Data base (NED) which is operated by the Jet Propulsion Laboratory, California Institute of Technology, under contract with the National Aeronautics and Space Administration. We acknowledge the usage of the HyperLeda data base (http://leda.univlyon1.fr). This research used the facilities of the Canadian Astronomy Data Centre operated by the National Research Council of Canada with the support of the Canadian Space Agency. Some of the data presented in this paper were obtained from the MAST. STScI is operated by the Association of Universities for Research in Astronomy, Inc., under NASA contract NAS5-26555. Support for MAST for non-*HST* data is provided by the NASA Office of Space Science via grant NNX09AF08G and by other grants and contracts.

We thank P.-A. Duc for kindly providing his proprietary CFHT+Megacam images of NGC 3389, and Giuliano Pignata for information on SN 2008bk. We also thank Luca Zampieri and Eddie Baron for useful discussions and advice. We thank the anonymous referee for the comments on the paper.

Downloaded from https://academic.oup.com/mnras/article-abstract/417/2/1417/984687
by Leiden University user
on 23 November 2017

REFERENCES

Abdel-Hamid H., Lee S.-G., Notni P., 2003, J. Korean Astron. Soc., 39, 54
Aldering G., Humphreys R. M., Richmond M., 1994, AJ, 107, 662
Asplund M., Grevesse N., Sauval A. J., Scott P., 2009, ARA&A, 47, 481
Benetti S. et al., 2001, MNRAS, 322, 361
Bessel M. S., 1979, PASP, 91, 589
Blondin S., Tonry J. L., 2007, ApJ, 666, 1024
Boissier S., Prantzos N., 2009, A&A, 503, 137
Bouchet P., Phillips M. M., Suntzeff N. B., Gouiffes C., Hanuschik R. W., Wooden D. H., 1991, A&A, 245, 490
Bresolin F., 2008, in Israelian G., Meynet G., eds, The Metal-Rich Universe. Cambridge Univ. Press, Cambridge, p. 155
Cardelli J. A., Clayton G. C., Mathis J. S., 1989, ApJ, 345, 245
Cohen M., Wheaton W. A., Megeath S. T., 2003, AJ, 126, 1090
Crockett R. M., Smartt S. J., Pastorello A., Stephens A. W., Maund J. R., Mattila S., 2011, MNRAS, 410, 2767
D'Andrea C. B. et al., 2010, ApJ, 708, 661
Dolphin A. E., 2000a, PASP, 112, 1383
Dolphin A. E., 2000b, PASP, 112, 1397
Dolphin A. E., 2009, PASP, 121, 655
Drilling J. S., Landolt A. U., 2000, in Cox A., ed., Allen's Astrophysical Quantities, 4th edn. Springer-Verlag, New York
Dwek E., 1983, ApJ, 274, 175
Eldridge J. J., Tout C. A., 2004, MNRAS, 353, 87
Eldridge J. J., Mattila S., Smartt S. J., 2007, MNRAS, 276, L52
Elias-Rosa N. et al., 2009, ApJ, 706, 1174
Filippenko A. V., 1999, IAU Circ. 7143
Fransson C., 1984, A&A, 132, 115
Gal-Yam A., Leonard D. C., 2009, Nat, 458, 865
Gustafsson B., Edvardsson B., Eriksson K., Jørgensen U. G., Nordlund Å., Plez B., 2008, A&A, 486, 951
Hamuy M., Pinto P. A., 2002, ApJ, 566, L63
Harutyunyan A. H. et al., 2008, A&A, 488, 383
Heger A., Fryer C. L., Woosley S. E., Langer N., Hartmann D. H., 2003, ApJ, 591, 288
Hendry M. A. et al., 2006, MNRAS, 369, 1303
Hodapp K. W. et al., 2003, PASP, 115, 1388
Johnson H. L., 1964, Boletin de los Observatorios de T. y T., 3, 305
Johnson H. L., 1966, ARA&A, 4, 449
Kasen D., Woosley S. E., 2009, ApJ, 703, 2205
Kirst J., Hook R., 2004, The Tiny Tim User's Manual. Space Telescope Science Institute, Baltimore, MD
Kitaura F. S., Janka H.-Th., Hillebrandt W., 2006, A&A, 450, 345
Landolt A. U., 1990, AJ, 104, 340
Levesque E. M., Massey P., Olsen K. A. G., Plez B., Josselin E., Maeder A., Meynet M., 2005, ApJ, 628, 973
Li W., Van Dyk S. D., Filippenko A. V., Cuillandre J.-C., 2005, PASP, 117, 121
Li W., Van Dyk S. D., Filippenko A. V., Cuillandre J.-C., Jha S., Bloom J. S., Riess A. G., Livio M., 2006, ApJ, 641, 1060
Maguire K., Kotak R., Smartt S. J., Pastorello A., Hamuy M., Bufano F., 2010a, MNRAS, 403, 11
Maguire K. et al., 2010b, MNRAS, 404, 981
Massey P., Plez B., Levesque E. M., Olsen K. A. G., Clayton G. C., Josselin E., 2005, ApJ, 634, 1286
Mattila S., Smartt S. J., Eldridge J. J., Maund J. R., Crockett R. M., Danziger I. J., 2008, ApJ, 688, L91
Maund J. R., Smartt S. J., 2009, Sci, 324, 286
Maund J. R., Smartt S. J., Danziger I. J., 2005, MNRAS, 364, L33
Meynet G., Maeder A., 2003, A&A, 404, 975
Moro D., Munari U., 2000, A&AS, 147, 361
Nakano S., 2009, Central Bureau Electronic Telegrams, 2065, 1
Pastorello A. et al., 2004, MNRAS, 347, 74
Pastorello A. et al., 2006, MNRAS, 370, 1752
Pastorello A. et al., 2009, MNRAS, 394, 2266
Poelarends A. J. T., Herwig F., Langer N., Heger A., 2008, ApJ, 675, 614
Poznanski D. et al., 2009, ApJ, 694, 1067
Poznanski D., Ganeshalingam M., Silverman J. M., Filippenko A. V., 2011, MNRAS, 415, L81
Pumo M. L. et al., 2009, ApJ, 705, L138
Schlegel D. J., Finkbeiner D. P., Davis M., 1998, ApJ, 500, 525
Siess L., 2006, A&A, 448, 717
Siess L., 2007, A&A, 476, 893
Skrutskie M. F. et al., 2006, AJ, 131, 1163
Smartt S. J., 2009, ARA&A, 47, 63
Smartt S. J., Eldridge J. J., Crockett R. M., Maund J. R., 2009, MNRAS, 395, 1409
Sollerman J., Ergon M., Inserra C., Valenti S., 2009, Central Bureau Electronic Telegrams, 2068, 1
Spillane T., Raiola F., Zeng S. et al., 2008, in Demetriou V. P., Julin R., Harissopulos S., eds, AIP Conf. Ser. Vol 1012, Frontiers in Nuclear Structure, Astrophysics, and Reactions: Finustar 2. Am. Inst. Phys., New York, p. 144
Spiro S., Pastorello A., 2009, in Giobbi G. et al., eds, AIP Conf. Ser. Vol. 1111, Probing Stellar Populations out to the Distant Universe. Am. Inst. Phys., New York, p. 460
Stancliffe R. J., Tout C. A., Puls O. R., 2004, MNRAS, 352, 984
Suntzeff N. B., Bouchet P., 1990, AJ, 99, 650
Terry J. N., Paturel G., Ekholm T., 2002, A&A, 393, 57
Tsujimoto T., Shigeyama T., 2003, ApJ, 584, L87
Tully R. B., 1988, Nearby Galaxies Catalog. Cambridge University Press, Cambridge
Turatto M. et al., 1998, ApJ, 498, L129
Turatto M., Benetti S., Cappellaro E., 2003, in Hillebrandt W., Leibundgut B., eds, From Twilight to Highlight: The Physics of Supernovae. Springer Berlin, Heidelberg
Utrobin V. P., 2007, A&A, 461, 233
Valenti S. et al., 2011, MNRAS, in press (doi:10.1111/j.1365-2966.2011.19262.x)
Waxman E., Draine B. T., 2000, ApJ, 537, 796
West R. M., Reipurth B., Jorgenson H. E., Cropper M., Bailey J. A., Peacock T. I., Wickramasinghe D. T., 1987, IAU Circ. 4319
White G. L., Malin D. F., 1987, IAU Circ. 4327
Woosley S. E., Weaver T. A., 1995, ApJS, 101, 181
Woosley S., Heger A., Weaver T., 2002, Rev. Mod. Phys., 74, 1015
Zampieri L., Pastorello A., Turatto M., Cappellaro E., Benetti S., Altavilla G., Mazzali P., Hamuy M., 2003, MNRAS, 338, 711

This paper has been typeset from a TEX/LATEX file prepared by the author.

Downloaded from https://academic.oup.com/mnras/article-abstract/417/2/1417/984687
by Leiden University user
on 23 November 2017